Fraunhofer Institut
Techno- und
Wirtschaftsmathematik

K. Schladitz, C. Redenbach, T. Sych, M. Godehardt

Microstructural characterisation of open foams using 3d images

Berichte des Fraunhofer ITWM, Nr. 148 (2008)

ISSN 1434-9973

Bericht 148 (2008)

Die Veröffentlichungen in der Berichtsreihe des Fraunhofer ITWM können bezogen werden über:

Fraunhofer-Institut für Techno- und
Wirtschaftsmathematik ITWM
Fraunhofer-Platz 1

67663 Kaiserslautern
Germany

Telefon: 06 31/3 16 00-0
Telefax: 06 31/3 16 00-10 99
E-Mail: info@itwm.fraunhofer.de
Internet: www.itwm.fraunhofer.de

Vorwort

Das Tätigkeitsfeld des Fraunhofer-Instituts für Techno- und Wirtschaftsmathematik ITWM umfasst anwendungsnahe Grundlagenforschung, angewandte Forschung sowie Beratung und kundenspezifische Lösungen auf allen Gebieten, die für Techno- und Wirtschaftsmathematik bedeutsam sind.

In der Reihe »Berichte des Fraunhofer ITWM« soll die Arbeit des Instituts kontinuierlich einer interessierten Öffentlichkeit in Industrie, Wirtschaft und Wissenschaft vorgestellt werden. Durch die enge Verzahnung mit dem Fachbereich Mathematik der Universität Kaiserslautern sowie durch zahlreiche Kooperationen mit internationalen Institutionen und Hochschulen in den Bereichen Ausbildung und Forschung ist ein großes Potenzial für Forschungsberichte vorhanden. In die Berichtreihe sollen sowohl hervorragende Diplom- und Projektarbeiten und Dissertationen als auch Forschungsberichte der Institutsmitarbeiter und Institutsgäste zu aktuellen Fragen der Techno- und Wirtschaftsmathematik aufgenommen werden.

Darüber hinaus bietet die Reihe ein Forum für die Berichterstattung über die zahlreichen Kooperationsprojekte des Instituts mit Partnern aus Industrie und Wirtschaft.

Berichterstattung heißt hier Dokumentation des Transfers aktueller Ergebnisse aus mathematischer Forschungs- und Entwicklungsarbeit in industrielle Anwendungen und Softwareprodukte – und umgekehrt, denn Probleme der Praxis generieren neue interessante mathematische Fragestellungen.

Prof. Dr. Dieter Prätzel-Wolters
Institutsleiter

Kaiserslautern, im Juni 2001

Microstructural characterisation of open foams using 3d images

Katja Schladitz, Claudia Redenbach, Tetyana Sych, Michael Godehardt

October 17, 2008

1 Introduction

Open cell foams are a promising and versatile class of porous materials. Open metal foams serve as crash absorbers and catalysts, metal and ceramic foams are used for filtering, and open polymer foams are hidden in every-day-life items like mattresses or chairs.

Due to their high porosity, classical 2d quantitative analysis can give only very limited information about the microstructure of open foams. On the other hand, micro computed tomography (μCT) yields high quality 3d images of open foams. Thus 3d imaging is the method of choice for open cell foams. In this report we summarise a variety of methods for the analysis of the resulting volume images of open foam structures developed or refined and applied at the Fraunhofer ITWM over a course of nearly ten years: The model based determination of mean characteristics like the mean cell volume or the mean strut thickness demanding only a simple binarisation as well as the image analytic cell reconstruction yielding empirical distributions of cell characteristics.

In Section 2 the intrinsic volumes and their densities serving as basic characteristics for cells and strut system, respectively, are introduced. Section 3 provides definitions and properties of both deterministic and random spatial tessellations. A choice of models particularly suited for solid foams is described in Section 4 including numerical values for the characteristics of the 'typical' cell needed for the model based analysis. Section 5 divides into three parts: Section 5.1 provides all image processing steps forming the cell reconstruction algorithm. Here, special attention is paid to the crucial prevention of over-segmentation by the watershed transform. Section 5.2 is dedicated to cell characteristics and their estimation. Recommendations for choosing the parameters for the two preferred methods substantiated by a simulation study are given in Section 5.3. Finally, limitations of the cell reconstruction method and a way out are illustrated on an example in the same section.

2 Intrinsic volumes and their densities

Foam cells are compact and in our context also convex subsets of the Euclidean space $\mathbb{R}^3$. We use the intrinsic volumes as a basic set of geometric characteristics for them. For finite unions of compact and convex sets $X \subset \mathbb{R}^3$ the intrinsic volumes V_j, $j = 0, \ldots, 3$ of X are – up to constant factors – the volume $V(X)$,

the surface area $S(X) = 2V_2(X)$, the integral of mean curvature $M(X) = \pi V_1(X)$, and the Euler number $\chi(X) = V_0(X)$, see e. g. [Sch93, p. 210].

Based on the isoperimetric inequalities [Sch93, pp. 318, 325], shape factors of three-dimensional objects X can be deduced from the intrinsic volumes:

$$f_1(X) = 6\sqrt{\pi}\frac{V(X)}{\sqrt{S(X)^3}}, \quad f_2(X) = 48\pi^2\frac{V(X)}{M(X)^3}, \quad f_3(X) = 4\pi\frac{S(X)}{M(X)^2}. \quad (1)$$

They are normalised such that $f_1(X) = f_2(X) = f_3(X) = 1$ for a ball X. Deviation from 1 describes various aspects of deviation from ball shape. We have $0 \leq f_1(X) \leq 1$ and for convex objects X also $0 \leq f_2(X), f_3(X) \leq 1$.

The strut system of open foams is described as a random closed subset of $\mathbb{R}^3$ (see e. g. [SKM95] or [SW08]), which is usually assumed to be stationary. Roughly speaking, the strut structure is in average the same, no matter where the sample/image is taken. More precisely, the distribution of X is translation invariant. Stationary random closed sets are characterised by the densities of the intrinsic volumes defined as the limit

$$V_{V,k}(X) = \lim_{r\to\infty} \frac{\mathbb{E}V_k(X \cap rW)}{V(rW)}, \qquad k = 0, \ldots, 3,$$

where $\mathbb{E}$ denotes expectation. Analogously to the intrinsic volumes, their densities have the following meaning: $V_V = V_{V,3}(X)$ is the volume density, $S_V = 2V_{V,2}(X)$ is the surface density (or specific surface area), $M_V = \pi V_{V,1}(X)$ is the density of the integral of the mean curvature, and $\chi_V = V_{V,0}(X)$ is the density of the Euler number.

The intrinsic volumes and their densities can be measured efficiently in binary images using discrete versions of the Crofton formula and the Euler-Poincaré formula as described in [SON06, OS08] and implemented in the 3D image analysis software MAVI [Fra05]. The densities of the intrinsic volumes (FieldFeatures in MAVI) are measured free of edge effects, whereas edge effects have to be dealt with when measuring intrinsic volumes of cells, faces, or struts. See Section 5.2 for a thorough account.

3 Tessellations

Tessellations are a class of models well suited for cellular materials such as foams, sintered materials like ceramics, or cellular biological structures. Roughly, a tessellation is a locally finite division of Euclidean space into bounded cells. Here, we restrict ourselves to the case of convex cells. Denote by $\mathring{C}$ the interior of the bounded set $C \subset \mathbb{R}^d$.

Definition 1 *Let T be a set of bounded convex d-dimensional subsets of $\mathbb{R}^d$ with*

1. *if $C_1, C_2 \in T$ and $C_1 \neq C_2$ then $\mathring{C}_1 \cap \mathring{C}_2 = \emptyset$,*
2. *$\bigcup_{C\in T} C = \mathbb{R}^d$,*
3. *T is locally finite, i.e. for every bounded Borel set $B \subset \mathbb{R}^d$ it holds that $\#\{C \in T : C \cap B \neq \emptyset\} < \infty$.*

Then T is called a tessellation *of $\mathbb{R}^d$.*

The cells are d-polytopes due to their convexity and the fact that the tessellation is space-filling [SW08, Lemma 10.1.1]. Denote by $\mathcal{F}^k(C)$ the set of all k-faces, $k = 0, \ldots, d$ of a d-polytope C.

Aiming at models for cellular materials we rule out unstable T-junctions in the tessellations. More precisely, faces of the tessellation should be faces of cells of the tessellation:

Definition 2 *Let T be a tessellation of $\mathbb{R}^d$. Write*

$$F(x) = \bigcap_{C \in T, x \in C} C, \quad x \in \mathbb{R}^d$$

for the intersection of all cells of T containing the point x. Then $F(x)$ is a non-empty finite intersection of d-polytopes and hence a k-polytope for some $k \in \{0, \ldots, d\}$. The set

$$\mathcal{F}^k(T) := \{F(x) : \dim F(x) = k, \quad x \in \mathbb{R}^d\} \quad k = 0, \ldots, d$$

is the set of k-faces of the tessellation T.

The tessellation T is called face-to-face *if the faces of the tessellation coincide with the faces of the cells:*

$$\mathcal{F}^k(T) = \bigcup_{C \in T} \mathcal{F}^k(C) \quad \textit{for} \quad k = 0, \ldots, d.$$

Normal tessellations or tessellations in the equilibrium state are of particular practical significance. This class of models is distinguished by the fact that – as for the microstructure of solid porous materials – almost surely four cells meet at every node and three cells meet at every edge.

Definition 3 *The tessellation T is called* normal *if*

$$F \in \mathcal{F}^k(T) \quad \textit{if and only if} \quad \#\{C \in T : C \cap F \neq \emptyset\} = d - k + 1.$$

All tessellation models considered in the following have convex cells, are normal and face-to-face. This rules out hyperplane processes for not being normal, Johnson-Mehl tessellations for having non-convex cells and the crack-STIT tessellation as well as nested tessellation models for not being face-to-face. Nevertheless, focusing on applications this is not a tight restriction as in practice solid cellular structures are normal and face-to-face. Often, the cell faces are slightly bent but for many structures convex cells are a good approximation.

3.1 Geometric properties of spatial tessellations

To describe the geometric properties of a spatial tessellation various counts can be used (e.g. the number of nodes etc.) as well as the geometric quantities for edges, polygons, and polyhedra like length, area, volume, etc. Due to the tessellation structure, there is a high degree of dependence between the characteristics. In this section, we provide two sets of parameters for normal tessellations and relations between the various characteristics, in particular those relating the two parameter sets to each other.

Additional to the densities of the intrinsic volumes we consider γ_k, $k \in \{0,1,2,3\}$ – the mean number of k-faces per unit volume – and the following characteristics of the 'typical k-face' of a tessellation:

N_{kl} denotes the mean number of l-faces adjacent to a k-face for $k,l \in \{0,1,2,3\}$, e. g. N_{13} denotes the mean number of cells neighbouring an edge ,
L_1 - the mean length of an edge,
L_2 - the mean perimeter of a face,
A_2 - the mean area of a face,
B_3 - the mean mean width of a cell,
L_3 - the mean total edge length of a cell,
S_3 - the mean surface area of a cell,
V_3 - the mean volume of a cell.

The typical k-face is a random polytope which, roughly speaking, has the same distribution as a randomly chosen k-face of the tessellation picked in such a way that every k-face has the same chance of being sampled. The precise definition using Palm distributions is due to Mecke [Mec80], see also [SW08].

3.1.1 Mean number of l-faces adjacent to a k-face

First we examine the dependencies of the N_{kl}. For every face-to-face tessellation of $\mathbb{R}^3$ we have

$$N_{10} = 2, \quad N_{23} = 2, \quad N_{20} = N_{21}, \quad \text{and} \quad N_{12} = N_{13}. \tag{2}$$

Euler's formula for the cell yields

$$N_{30} - N_{31} + N_{32} = 2 \tag{3}$$

while Euler's formula applied to the intersection of a sphere of suitable radius with all edges, faces, and cells adjacent to a vertex gives

$$N_{01} - N_{02} + N_{03} = 2,$$

see [JJCL04]. Multiple counting of the edges of a cell and the faces adjacent to a vertex, respectively, yields

$$\begin{aligned} 2N_{31} &= N_{32}N_{21} \quad \text{and} \\ 2N_{02} &= N_{01}N_{12}. \end{aligned} \tag{4}$$

Normality yields additionally:

$$N_{kl} = \binom{4-k}{l-k}, \quad k \le l.$$

That is

$$\begin{aligned} &N_{03} = 4, \quad N_{02} = 6 \quad \text{and} \quad N_{01} = 4, \\ &N_{13} = 3, \quad N_{12} = 3, \\ &N_{23} = 2. \end{aligned} \tag{5}$$

Now $N_{01} = 4$ implies in turn that three edges of a cell meet in a vertex and thus multiple counting of the vertices of a cell yields

$$3N_{30} = 2N_{31}.$$

Combined with the Euler formula (3) this gives

$$N_{30} = 2(N_{32} - 2) \quad \text{and} \quad N_{31} = 3(N_{32} - 2),$$

which leads together with (4) and (2) to

$$N_{20} = N_{21} = 6 - \frac{12}{N_{32}}.$$

Summing up, for normal tessellations we end up with just one of the $N_{kl}, \quad k > l$, as free parameter and we choose N_{32}.

3.1.2 The mean number of k-faces per unit volume

The general multiple counting result [SW08, Theorem 10.1.2]

$$\gamma_k N_{kl} = \gamma_l N_{lk} \quad \text{for} \quad k, l = 0, 1, 2, 3, \ k \neq l \tag{6}$$

combined with (2) and (5) yields

$$\gamma_1 = \gamma_0 \frac{N_{01}}{N_{10}} = 2\gamma_0 \ . \tag{7}$$

Furthermore, we have $\gamma_0 - \gamma_1 + \gamma_2 - \gamma_3 = 0$ [SW08, Theorem 10.1.3] due to Gram's relation which is an angle sum relation for polyhedral sets similar to Euler's relation. Thus

$$\gamma_2 = \gamma_0 + \gamma_3 \ . \tag{8}$$

Consider now the edge system of the tessellation T only. Following [SW08, Definition 10.1.4] we call

$$Z_1 := \bigcup_{C \in T} \mathcal{F}^0(C) \cup \bigcup_{C \in T} \mathcal{F}^1(C)$$

the 1-skeleton of T. For the specific Euler number of this 1-skeleton we have [SW08, Theorem 10.1.8]

$$\chi_V(Z_1) = \gamma_0 - \gamma_1,$$

which reduces in the normal case by (7) to

$$\chi_V(Z_1) = -\gamma_0. \tag{9}$$

3.1.3 Mecke's parameters

Mecke developed a parameter system using three parameters for tessellations of $\mathbb{R}^2$ and seven parameters for tessellations of $\mathbb{R}^3$, reducing to two and four parameters for normal tessellations, respectively. In $\mathbb{R}^3$, these parameters are [SKM95]:

γ_0 - the mean number of nodes per unit volume,

γ_3 - the mean number of cells per unit volume,

L_V - the mean total edge length per unit volume,

S_V - the mean total surface area of cells per unit volume.

The other characteristics of spatial normal tessellations can be obtained by the following relations:

$$
\begin{aligned}
N_{32} &= \frac{N_{23}\gamma_2}{\gamma_3} = \frac{2(\gamma_0+\gamma_3)}{\gamma_3}, && (10)\\
L_1 &= \frac{L_V}{\gamma_1} = \frac{L_V}{2\gamma_0},\\
L_2 &= \frac{N_{12}L_V}{\gamma_2} = \frac{3L_V}{\gamma_0+\gamma_3},\\
A_2 &= \frac{S_V}{\gamma_2} = \frac{S_V}{\gamma_0+\gamma_3},\\
L_3 &= \frac{N_{13}L_V}{\gamma_3} = \frac{3L_V}{\gamma_3},\\
B_3 &= \frac{L_V}{4\gamma_3}, && (11)\\
S_3 &= \frac{N_{23}S_V}{\gamma_3} = \frac{2S_V}{\gamma_3}, && (12)\\
V_3 &= \frac{1}{\gamma_3}. && (13)
\end{aligned}
$$

The formula for the mean width of the typical cell (11) follows from the following result for the integral of mean curvature M_3 of the typical cell [SW08, Theorem 10.1.7],

$$B_3 = \frac{1}{2\pi}M_3 = \frac{1}{4}\frac{\gamma_2}{\gamma_3}L_2 - \frac{1}{2}\frac{\gamma_1}{\gamma_3}L_1 = \frac{L_V}{\gamma_3}\left(\frac{3}{4}-\frac{1}{2}\right).$$

Hence for fixed γ_3 the values of S_3 and B_3 are proportional to S_V and L_V, respectively, and N_{32} only depends on γ_0.

3.1.4 Cell based parameters

For model-fitting based on image data and simulations, another set of parameters using characteristics of the typical cell turns out to be more practical:

V_3 - the mean volume of the typical cell,

S_3 - the mean surface area of the typical cell,

B_3 - the mean mean width of the typical cell,

N_{32} - the mean number of faces of the typical cell.

We use the sphericity f_1 from (1) as additional information on the regularity of the cells.

The cell based parameter set has two advantages. First, simulated tessellations are described by means of analytic geometry – real valued coordinates for generators and vertices as well as line and plane equations for edges and faces. Comparison to real structures demands discretisation. The cell characteristics are less effected by discretisation effects than e. g. L_V. Second, and more important, mean values are not sufficient for model-fitting. At least empirical variances have to be estimated, too. See [Lau08]. Using characteristics of the

cells allows estimation of empirical distributions and thus provides the information needed for model fitting. However, contrary to the first set of parameters, estimation of the cell characteristics is hampered by edge effects. See Section 5.2 below for correction methods.

Mecke's parameters are computed from the second parameter set using the following equations:

$$\begin{aligned} \gamma_0 &= \frac{N_{32} - 2}{2V_3}, \\ \gamma_3 &= \frac{1}{V_3}, \\ L_V &= \frac{4B_3}{V_3}, \\ S_V &= \frac{S_3}{2V_3}. \end{aligned}$$

These equations follow directly from (10), (11), and (12) using (13).

3.2 Tessellation models

3.2.1 Voronoi tessellations

Voronoi tessellations are the mathematical model capturing the natural idea of dividing space into influence zones given a set of generators.

Definition 4 *Let $\varphi = \{x_1, x_2, \ldots\} \subseteq \mathbb{R}^d$ be a locally finite set of generators. Assign each point $x \in \varphi$ the set $C(x)$ of those points in space having a smaller distance to this point than to any other point $y \in \varphi$. The* Voronoi cell $C(x)$ *is given by*

$$C(x) := \{z \in \mathbb{R}^3 \,:\, ||z - x|| \leq ||z - y|| \text{ for all } y \neq x,\, y \in \varphi\}, \quad x \in \varphi,$$

where $||\cdot||$ denotes the Euclidean norm in $\mathbb{R}^d$. The Voronoi tessellation *of $\mathbb{R}^d$ w. r. t. φ is the set of all Voronoi cells generated by the points in φ*

$$T(\varphi) = \{C(x) :\ x \in \varphi\}.$$

3.2.2 Laguerre tessellations

Laguerre tessellations are a generalisation of the Voronoi case. The Euclidean distance is replaced by the so-called power distance.

Definition 5 *For $y, x \in \mathbb{R}^d$ and $r \geq 0$ define the* power of y w. r. t. the pair (x, r) *as*

$$\text{pow}\big(y, (x, w)\big) := ||y - x||^2 - r^2.$$

Often the pair (x,r) is identified with a sphere in $\mathbb{R}^d$ with centre x and radius r.

Let $\varphi \subset \mathbb{R}^d \times \mathbb{R}$ be a countable set such that $\min_{(x,r)\in\varphi} \text{pow}\,(y, (x, r))$ exists for each $y \in \mathbb{R}^d$. Then the Laguerre cell *of $(x, r) \in \varphi$ is defined as*

$$C\big((x, r), \varphi\big) := \{y \in \mathbb{R}^d \,:\, \text{pow}\,\big(y, (x, r)\big) \leq \text{pow}\,\big(y, (x', r')\big), \quad (x', r') \in \varphi\}.$$

The point x is called the nucleus of the cell $C\big((x, r), \varphi\big)$.

The Laguerre diagram $L(\varphi)$ *is the set of the non-empty Laguerre cells of* φ*, i.e.*

$$L(\varphi) := \{C((x,r),\varphi) \,:\, (x,r) \in \varphi, C((x,r),\varphi) \neq \emptyset\}.$$

The significance of Laguerre tessellations arises from the fact that each normal face-to-face tessellation of $\mathbb{R}^d$ for $d > 2$ with convex cells is a Laguerre tessellation [Aur87, Lau07].

3.2.3 Lattice based structures

The 3d microstructure of polymer foams often shows a strong prevalence of pentagonal cell faces leading to the widespread belief that the perfect foam consists of regular pentagonal dodecahedra. However, even if the regularity assumption is relaxed, there is no space-filling and face-to-face tessellation with pentagonal dodecahedra.

The most prominent deterministic foam model is Kelvin's foam consisting of congruent truncated octahedra [Wea96]. This is the Voronoi tessellation generated by the bcc lattice. Its successor, the Weaire-Phelan foam [Wea96] is more suited for modelling solid foams as its cells are (non-regular) pentagonal dodecahedra and tetradecahedra having two hexagonal and 12 pentagonal faces. Dodecahedra and tetradecahedra appear in the proportion 1:3. In general, the Weaire-Phelan foam is defined w. r. t. a parameter α. Here, we consider just the case of equal-volume cells and planar faces which corresponds to the choice $\alpha = \sqrt[3]{2}$. For this case, the geometric characteristics of the cells were computed in [Syc04].

For the dodecahedra we have

$$N_{32} = 12, \quad N_{31} = 30, \quad N_{30} = 20.$$

If the dodecahedron is centred at the origin, a face P_1 is given by the coordinates of the vertices:

$$A_1 = \left(0, -\frac{\alpha}{2}, \alpha\right), A_2 = \left(0, \frac{\alpha}{2}, \alpha\right), A_3 = \left(\frac{2}{3}\alpha, \frac{2}{3}\alpha, \frac{2}{3}\alpha\right),$$
$$A_4 = \left(\alpha, 0, \frac{\alpha}{2}\right), A_5 = \left(\frac{2}{3}\alpha, -\frac{2}{3}\alpha, \frac{2}{3}\alpha\right).$$

Now simple analytic geometry yields perimeter length and area of this face. The volume of the dodecahedron is obtained by splitting it into congruent pyramids. We get

$$\begin{aligned} L_3 &= 6\sqrt[3]{2}(1 + 2\sqrt{\frac{7}{3}}) \approx 30.654, \\ S_3 &= 6\sqrt[3]{4}\sqrt{5} \approx 21.297, \quad \text{and} \\ V_3 &= 8. \end{aligned}$$

For the tetradecahedra we have

$$N_{32} = 14, \quad N_{31} = 36, \quad N_{30} = 24.$$

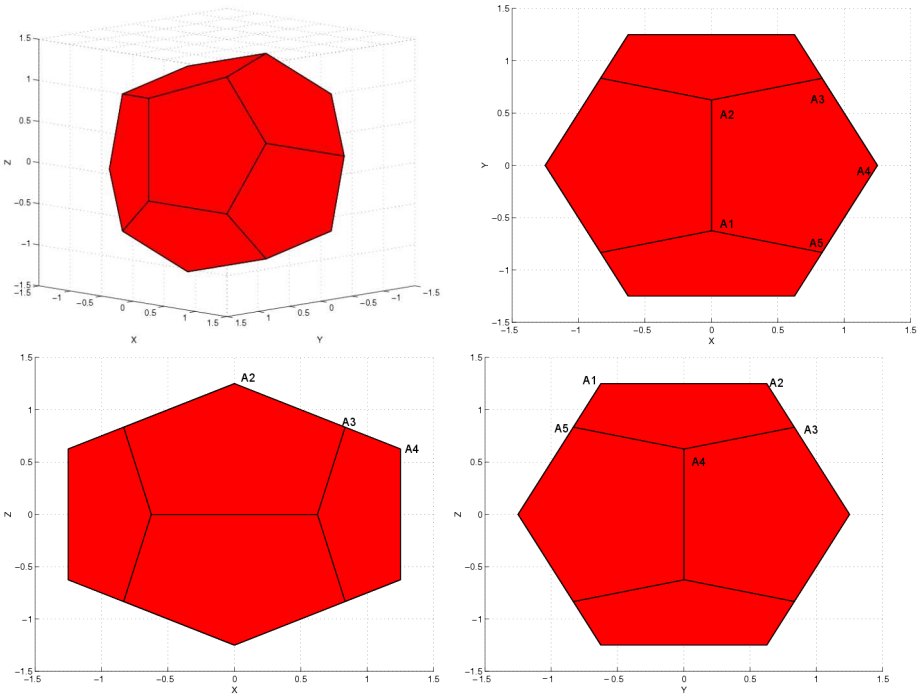

Figure 1: Dodecahedral cell of the Weaire-Phelan foam, 3d view and projections onto the three coordinate planes.

There are four faces of type P_1, 8 faces of type P_2, and two hexagonal faces. A P_2-pentagon is given by the vertices

$$B_1 = \left(\frac{2}{3}\alpha - 1, \frac{2}{3}\alpha, 2 - \frac{2}{3}\alpha\right), B_2 = \left(1 - \frac{2}{3}\alpha, 2 - \frac{2}{3}\alpha, \frac{2}{3}\alpha\right), B_3 = \left(1, 2 - \alpha, \frac{\alpha}{2}\right),$$
$$B_4 = (1, 0, 1), B_5 = \left(\alpha - 1, 0, 2 - \frac{\alpha}{2}\right).$$

A hexagonal face has the vertices

$$C_1 = \left(1, 2 - \alpha, \frac{\alpha}{2}\right), C_2 = \left(1, 2 - \alpha, -\frac{\alpha}{2}\right), C_3 = (1, 0, -1),$$
$$C_4 = \left(1, -(2 - \alpha), -\frac{\alpha}{2}\right), C_5 = \left(1, -(2 - \alpha), \frac{\alpha}{2}\right), C_6 = (1, 0, 1).$$

For the tetradecahedron this leads to

$$\begin{aligned} L_3 &= 6(2 - \sqrt[3]{2})\sqrt{5} + 4(\sqrt[3]{2} + 2\sqrt{\frac{7}{3}}) + 4\frac{4 - \sqrt[3]{2}}{\sqrt{3}} \approx 32.583, \\ S_3 &= 2\sqrt[3]{4}(\sqrt{5} - 4\frac{\sqrt{6}}{3} - 1) + 8(1 + \sqrt{6}) \approx 21.151, \quad \text{and} \\ V_3 &= 8. \end{aligned}$$

Finally, normalising to $V_3 = 1$ and averaging yields the characteristics of the 'typical cell'

$$N_{32} = 13.5 \quad L_3 \approx 16.050 \quad S_3 \approx 5.297 \quad f_1 \approx 0.872.$$

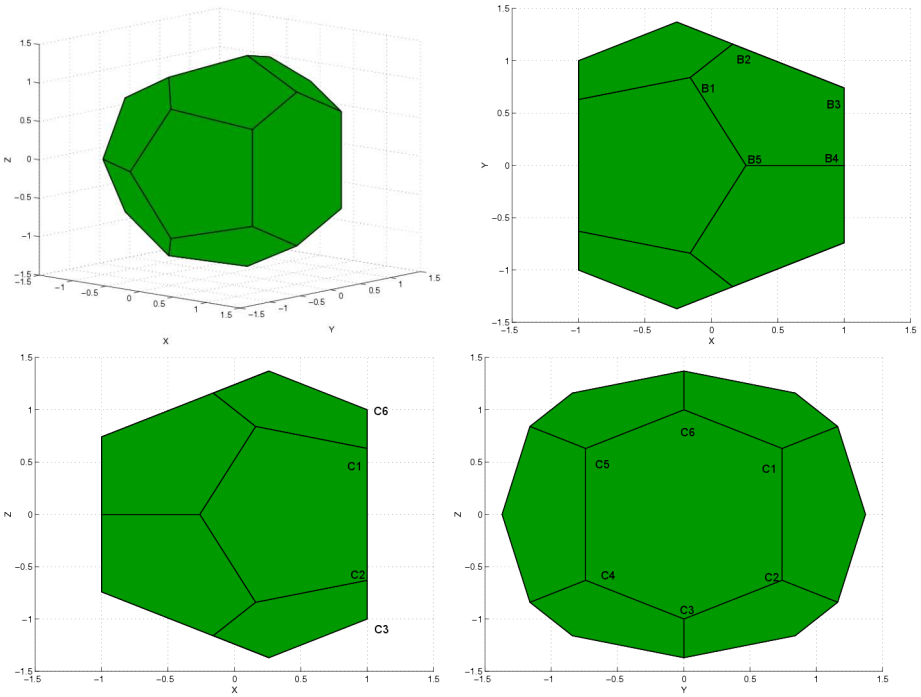

Figure 2: Tetradecahedral cell of the Weaire-Phelan foam, 3d view and projections onto the three coordinate planes.

Example 1 *The mean number characteristics for the monohedral tessellations by cubes and hexagonal prisms and for the Kelvin and Weaire-Phelan foams are given in Table 1.*

	cubes			Kelvin			Weaire-Phelan		
vertices	N_{01}	N_{02}	N_{03}	N_{01}	N_{02}	N_{03}	N_{01}	N_{02}	N_{03}
	6	12	8	4	6	4	4	6	4
edges	N_{10}	N_{12}	N_{13}	N_{10}	N_{12}	N_{13}	N_{10}	N_{12}	N_{13}
	2	4	4	2	3	3	2	3	3
faces	N_{20}	N_{21}	N_{23}	N_{20}	N_{21}	N_{23}	N_{20}	N_{21}	N_{23}
	4	4	2	$\frac{36}{7}$	$\frac{36}{7}$	2	$\frac{46}{9}$	$\frac{46}{9}$	2
cells	N_{30}	N_{31}	N_{32}	N_{30}	N_{31}	N_{32}	N_{30}	N_{31}	N_{32}
	8	12	6	24	36	14	23	$\frac{69}{2}$	$\frac{27}{2}$

Table 1: Deterministic tessellations of $\mathbb{R}^3$. Mean values for geometric characteristics of vertices, edges, faces, and cells.

The Weaire-Phelan foam has the desired high proportion of pentagonal faces. However, deterministic models are not able to capture the microscopic heterogeneity of real foams. Moreover, for some fields of application like filtration, a certain degree of heterogeneity seems to be favourable. Therefore we move on to random tessellations.

3.3 Random tessellations

Real solid foams are regular structures but show microscopic heterogeneity of varying degree, too. The models introduced in Section 3.2 can easily be randomised by choosing randomly distributed generators (and weights in the Laguerre case).

For the generators we use spatial random point processes and random packings of balls. The first are roughly speaking locally finite random point patterns, see e. g. [SKM95], while the latter are defined by the packing algorithm used. Here we consider only packings obtained by the force biased procedure, see [BBS02] and the references therein.

3.3.1 Poisson Voronoi tessellation

The stationary Poisson point process describes a perfectly random point pattern: The numbers of points in disjoint sets are independent random variables and given their number the points in a compact set are i. i. d. uniformly. Consequently, the points are in general position. That is, almost surely no three points lie on a straight line and no five points lie on a sphere. Due to the latter, Poisson Voronoi tessellations are normal [SW08, Theorem 10.2.3].

For the Poisson Voronoi tessellation, the only degree of freedom is the intensity λ of the generating Poisson point process. That is, the mean number of points per unit volume. From λ, all four parameters of the tessellation can be deduced:

$$\begin{aligned}
\gamma_0 &= \frac{24}{35}\pi^2\lambda \\
\gamma_3 &= \lambda \\
L_V &= \frac{16}{15}\left(\frac{3}{4}\right)^{\frac{1}{3}}\pi^{\frac{5}{3}}\Gamma\left(\frac{4}{3}\right)\lambda^{\frac{2}{3}} \approx 5.83\lambda^{\frac{2}{3}} \\
S_V &= 4\left(\frac{\pi}{6}\right)^{\frac{1}{3}}\Gamma\left(\frac{5}{3}\right)\lambda^{\frac{1}{3}}.
\end{aligned}$$

For the second set of parameters we get:

$$\begin{aligned}
B_3 &= \frac{4}{15}\left(\frac{3}{4}\right)^{\frac{1}{3}}\pi^{\frac{5}{3}}\Gamma\left(\frac{4}{3}\right)\lambda^{-\frac{1}{3}} \approx 1.458\lambda^{-\frac{1}{3}} \\
S_3 &= 8\left(\frac{\pi}{6}\right)^{\frac{1}{3}}\Gamma\left(\frac{5}{3}\right)\lambda^{-\frac{2}{3}} \approx 5.821\lambda^{-\frac{2}{3}} \\
V_3 &= \lambda^{-1} \\
N_{32} &= 2\left(\frac{24}{35}\pi + 1\right) \approx 15.535.
\end{aligned}$$

The sphericity can only be obtained by simulations $f_1 \approx 0.728$, see [Lau07, LH93].

3.3.2 Hard-core Voronoi tessellation

For applications, Poisson Voronoi tessellations are often too irregular, as cellular structures in both biology and materials science often have a certain minimum

size due to the generation process and show a certain degree of regularity not just w. r. t. cell size but w. r. t. cell shape, too. Therefore, Voronoi tessellations generated by a hard-core point field are more realistic. However, these tessellations are no longer analytically tractable and thus their geometric characteristics have to be determined by simulation.

The Matérn hard-core model II with hard-core radius R is obtained by thinning a Poisson point process: The points are furnished with an i. i. d. mark (for instance date of birth or size). If two points are closer than R, then the point with lower mark is removed. In [LH93] simulation results for the Voronoi tessellation w. r. t. a Matérn hard-core II point field with intensity 1 and hard-core radius $R_{hc} = 0.124$ are reported, see also [OM00]:

$$N_{32} = 15.335 \quad L_3 = 17.178 \quad S_3 = 5.703 \quad f_1 = 0.772.$$

3.3.3 Poisson Laguerre tessellations

Laguerre tessellations generated by stationary marked Poisson processes are a generalisation of Poisson Voronoi tessellations allowing to incorporate knowledge about the cell sizes into the model as the structure of these tessellations depends on both the intensity λ of the generating Poisson process and the mark distribution. Similar to the Poisson Voronoi case it can be shown that Poisson Laguerre tessellations are normal [LZ08]. Furthermore, integral formulae for various mean values as well as contact distributions can be derived and evaluated numerically. In 3d, these formulae include for instance γ_0, L_V, and S_V.

Laguerre cells can be empty, therefore the cell intensity γ_3 does not necessarily equal the intensity of the generating Poisson process. A formula for γ_3 can nevertheless be obtained. However, it is not tractable to numerical evaluation. Consequently, characteristics of the typical cell have to be determined by simulations. For details on Poisson Laguerre tessellations we refer to [LZ08, Lau07].

3.3.4 Laguerre tessellations generated by random packings of balls

As in the special case of the Voronoi tessellation, Poisson Laguerre tessellations turn out to be too irregular in order to provide realistic models for foam structures. A better choice are Laguerre tessellations generated by random dense packings of balls which yield more regular cell structures.

For applications, the possibility to create cells with a given size distribution is highly important. Not only can models be fitted much better, it is even possible to include knowledge about the origin of the structure to be modelled into the model fit. In [FWZL04] it was shown that the cell volume distribution in a Laguerre tessellation generated by a dense packing of balls is closely determined by the volume distribution of the generating balls. Since lognormal and gamma distributions are often considered good models for the size distribution of the cells in cellular materials, it seems reasonable to work with one of these distribution families.

Here, simulation results for two Laguerre tessellations based on force biased packings with lognormal distribution of the ball volumes are reported. The balls are packed rather densely ($V_V = 60\%$) in order to achieve a very regular cell structure. Aiming at $V_3 = 1$ we choose the mean ball size 0.6 leaving the coefficient of variation (cv) of the ball size as the free parameter. For $cv = 0.2$

we get model L1 with

$$N_{32} = 14.145 \quad L_3 = 16.302 \quad S_3 = 5.368 \quad f_1 = 0.850$$

while $cv = 2.0$ yields model L2 with

$$N_{32} = 13.371 \quad L_3 = 15.186 \quad S_3 = 4.908 \quad f_1 = 0.800.$$

For details we refer to [Red08].

Note that normality of the resulting Laguerre tessellations is not guaranteed since no general position property for the generating balls placed by the force biased algorithm can be proved. In the realizations however, no deviations from normality have been observed.

3.3.5 Random perturbations of the Weaire-Phelan foam

The Weaire-Phelan foam from Section 3.2.3 is a normal face-to-face tessellation of $\mathbb{R}^3$ in convex cells and thus a Laguerre tessellation, too. The set of generating spheres is given by the cell centres where the spheres generating dodecahedra have radius 0 while the generators of tetradecahedra have radius $R = \sqrt{4\sqrt[3]{2} - 5}$. This description is used in [LS08] for random perturbation of this deterministic model by slightly changing both the generators and the weights.

It turned out that a large disturbance of the radii tends to destroy the structure of the tessellation since a lot of cells is deleted. Shifting the positions of the sphere centres results in tessellations with a decreasing degree of regularity. The mean values of the number of faces per cell even approach the values which are observed for Laguerre tessellations generated by Poisson processes, see [Lau07].

Before deducing mean values of geometric characteristics for open foams based on the models we summarise the cell characteristics for the Poisson Voronoi (PV), the Weaire-Phelan (WP), the Matérn hard-core Voronoi (HCV), and the two Laguerre tessellations (L1 and L2) described above in Table 2.

	PV	HCV	L1	L2	WP
γ_0	6.768	6.668	6.072	5.686	5.75
L_V	5.832	5.728	5.436	5.064	5.352
S_V	2.910	2.852	2.684	2.454	2.648
N_{32}	15.535	15.335	14.145	13.371	13.5
L_3	17.496	17.178	16.302	15.186	16.050
S_3	5.821	5.703	5.368	4.908	5.297
B_3	1.458	1.432	1.359	1.266	1.338
f_1	0.728	0.772	0.850	0.800	0.872

Table 2: The two parameter sets for the Poisson Voronoi (PV), the Weaire-Phelan (WP), the Matérn hard-core Voronoi (HCV), and the two Laguerre tessellations (L1 with $cv = 0.2$ and L2 with $cv = 2.0$), normalised to $V_3 = 1$, $\gamma_3 = 1$.

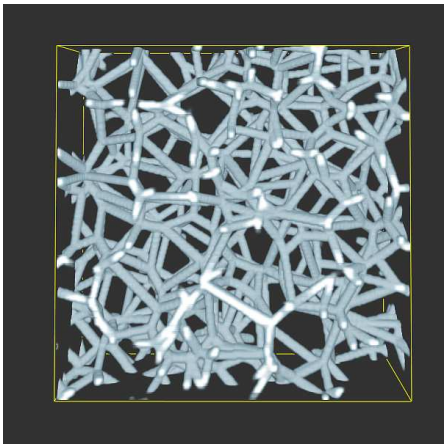

(a) Poisson Voronoi tessellation

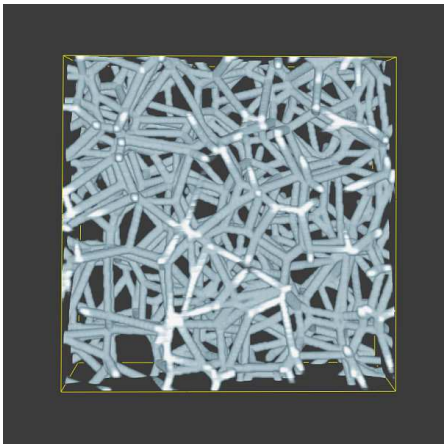

(b) Hard-core Voronoi tessellation

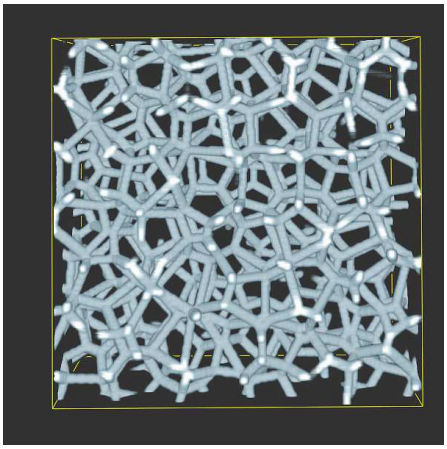

(c) Laguerre tessellation L1

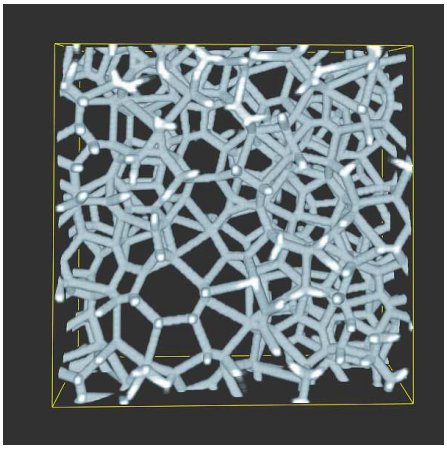

(d) Laguerre tessellation L2

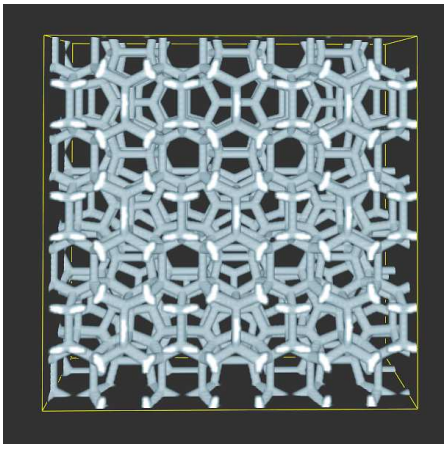

(e) Weaire-Phelan foam

Figure 3: Volume renderings of dilated edge systems of tessellation models.

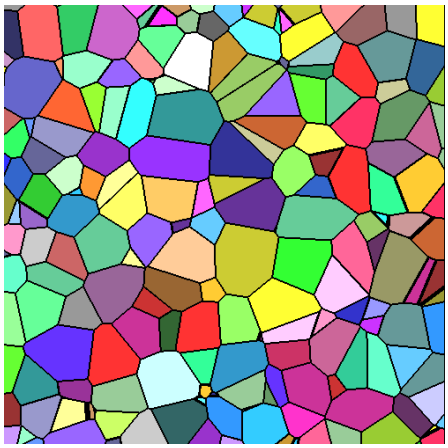

(a) Poisson Voronoi tessellation

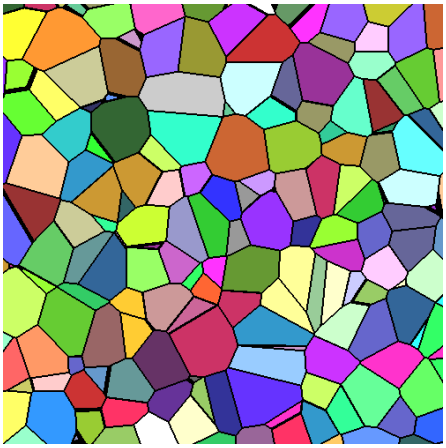

(b) Hard-core Voronoi tessellation

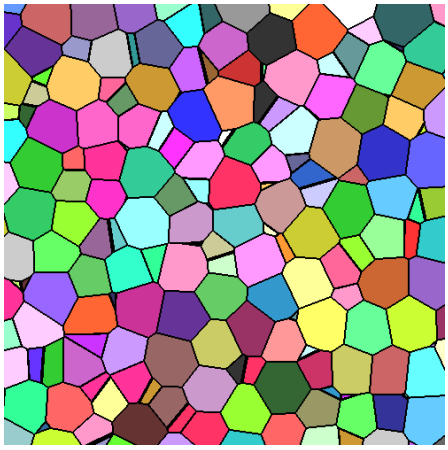

(c) Laguerre tessellation L1

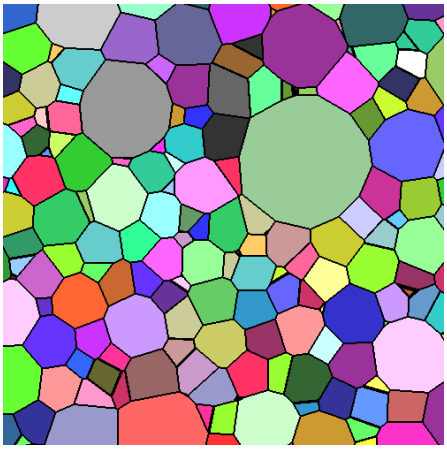

(d) Laguerre tessellation L2

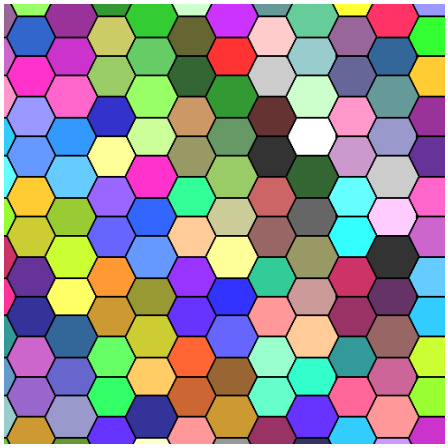

(e) Weaire-Phelan foam

Figure 4: 2d slices through the cell system of 3d tessellation models.

4 Mean values of geometric characteristics for open foams

As mentioned in Section 2, the strut system of open foams can be described as a spatially homogeneous random closed set.

When measuring characteristics of the strut system, a specific surface area different from S_V of the tessellation is determined. In order to avoid confusion, we write S_V^{struts} for the specific surface area of the strut system opposed to the specific surface area of the tessellation S_V.

The following characteristics specific for open foams can be deduced from the densities of the intrinsic volumes:

p – the porosity $1 - V_V$,

L_V – die specific strut length (mean total length per unit volume)

$$L_V \approx \frac{M_V}{\pi\,(1 - V_V)}, \tag{14}$$

γ_0 – the intensity of nodes $\gamma_0 = -\chi_V$

$\overline{u}$ – the mean strut perimeter $\overline{u} = \frac{S_V^{\text{struts}}}{L_V}$,

$\overline{\overline{b}}$ – the mean diameter of the struts $\overline{\overline{b}} = \frac{S_V^{\text{struts}}}{\pi\, L_V}$ and

$\overline{a}$ – the mean cross section area of the struts $\overline{a} = \frac{V_V}{L_V}$.

Division by the porosity in (14) corrects for the loss of total strut length at the nodes. The thicker the struts get the more strut length is ignored by the integral of mean curvature due to overlapping of the struts at the nodes. The equation for the node-intensity follows from (9) since solid open foams can be modelled as the (dilated) system of the edges of a normal tessellation.

The mean chord length $\widetilde{\ell}$ is of special interest in quality control of the production of open foams. It corresponds to the ppi-value (the mean number of pores per inch) which is used in various industrial standards:

$$\text{ppi} = \frac{1}{\widetilde{\ell}[\text{inch}]}.$$

Given the tessellation model, the characteristics of the typical cell are known up to a scaling factor. This scaling factor k is determined from the binary image of the edges by either using

$$L_V = \frac{1}{k^2} L_V^{(m)} \tag{15}$$

or

$$\chi_V = \frac{1}{k^3} \chi_V^{(m)}, \tag{16}$$

where $L_V^{(m)}$ and $\chi_V^{(m)}$ denote the specific strut length and the Euler number density of the model structure normalised to $V_3^{(m)} = 1$. Now cell and node

pixel size	strut diameter [pixel]	L_V	$\widehat{k}_L$	χ_V	$\widehat{k}_\chi$
L2 (10 000 cells)					
analytic		2349	1.001	−56 886	1.001
1/900	1	2077	1.063	−55 364	1.009
1/700	1	1982	1.088	−54 598	1.013
1/500	1	1817	1.137	−53 181	1.022
1/500	5	1163	1.421	−47 685	1.060
1/500	10	485	2.202	−42 087	1.106
1/500	15	100	4.840	−39 021	1.134
PV (10 043 cells)					
analytic		2715	0.998	−67 847	0.998
1/1000	1	2372	1.070	−67 833	1.000
1/1000	5	1854	1.210	−60 087	1.041
1/1000	10	1451	1.368	−54 657	1.075
1/1000	15	1282	1.455	−51 439	1.090
1/500	1	1974	1.173	−62 133	1.030
1/500	5	1461	1.363	−54 584	1.075
1/500	10	1009	1.640	−46 455	1.135
1/500	15	366	2.724	−35 557	1.240

Table 3: Estimated L_V and χ_V and the deduced estimates for the scaling factor k for the models L2 and PV for several resolutions and strut diameters. "Analytic" is measured directly from the description of the realization as set of nodes and edges.

densities as well as the specific surface area are deduced from the corresponding quantities for the chosen model

$$\gamma_3 = \frac{1}{k^3}\gamma_3^{(m)} \qquad \gamma_0 = \frac{1}{k^3}\gamma_0^{(m)} \qquad S_V = \frac{1}{k}S_V^{(m)}.$$

Similarly we get for the means of volume, surface area, mean width, edge length, and number of faces of the typical cell

$$V_3 = k^3 \qquad S_3 = k^2 S_3^{(m)} \qquad B_3 = kB_3^{(m)} \qquad L_3 = kL_3^{(m)} \qquad N_{32} = N_{32}^{(m)}.$$

Here the characteristics of the model are denoted by the superscript (m).

The influence of the model assumption on these parameters is relatively small, as all are mean values. The simulation study in [LS06] shows that the error due to the wrong model assumption is negligible compared to the error due to discretisation/resolution.

A simulation study using the Laguerre tessellation model L2 and a Poisson Voronoi tessellation with different strut thicknesses and on different resolutions showed that the scaling factor should be deduced from (16) since the specific strut length is underestimated due to the overlap of struts at the nodes. Consequently, the estimation error increases with increasing strut thickness and decreasing resolution.

The relatively small differences between the results under the different model assumptions are reassuring when determining the open foam characteristics. On the other hand, they show also, that just using first order characteristics can not suffice for fitting models to foams.

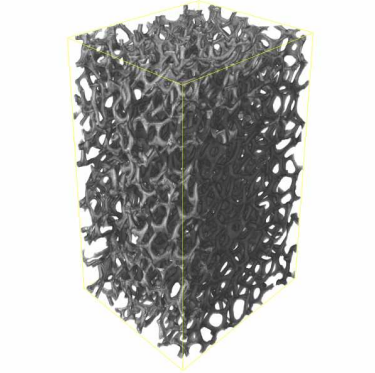

(a) Nickel foam, pixel size 10μm, visualised are $140 \times 140 \times 200$ pixels corresponding to $1.4 \times 1.4 \times 2\text{mm}^3$. μCT imaging Fraunhofer IZFP.

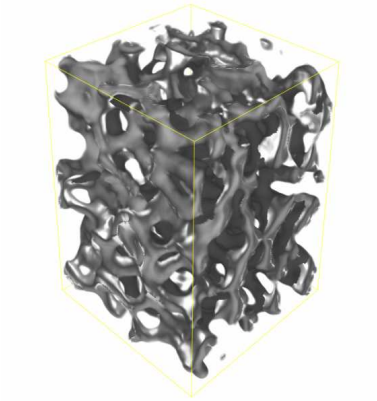

(b) Nickel-chrome foam, pixel size 12μm, visualised are $117 \times 117 \times 167$ pixels corresponding to $1.4 \times 1.4 \times 2\text{mm}^3$. μCT imaging RJL Micro & Analytic, sample Recemat International (RCM-NC-4753.05)

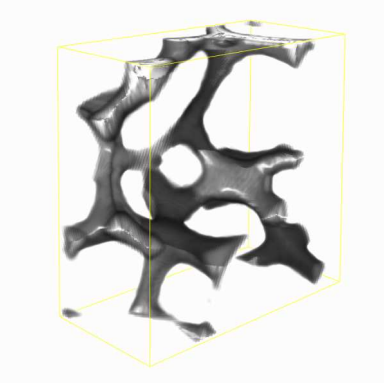

(c) Aluminium foam, pixel size 74.25μm, visualised are $97 \times 48 \times 97$ pixels corresponding to $7.2 \times 3.6 \times 7.2\text{mm}^3$. μCT imaging Fraunhofer IZFP, sample m-pore.

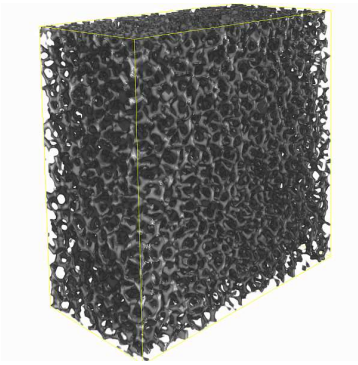

(d) Nickel-chrome foam from (b), $600 \times 300 \times 600$ pixels corresponding to $7.2 \times 3.6 \times 7.2\text{mm}^3$.

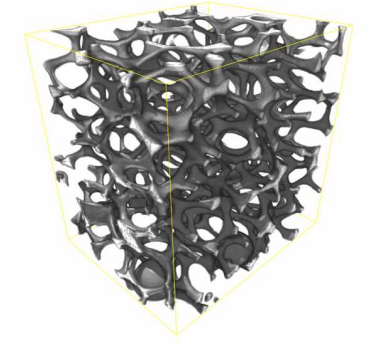

(e) Aluminium foam from (c), $251 \times 220 \times 380$ pixels corresponding to $18 \times 16 \times 28\text{mm}^3$.

Figure 5: Reconstructed tomographic images of open foam samples, (b) and (d) as well as (c) and (e) show different sample sizes of the same foam, respectively.

	unit	PV	HCV	L1	L2	WP
nickel foam						
γ_3	mm^{-3}	16.384	16.630	18.260	19.502	19.283
V_3	mm^3	0.061	0.060	0.055	0.051	0.052
S_3	mm^2	0.902	0.875	0.774	0.677	0.737
B_3	mm	0.574	0.561	0.516	0.470	0.499
γ_2	mm^{-3}	127.3	127.5	129.1	130.4	130.2
A_2	mm^2	0.058	0.057	0.055	0.051	0.055
γ_1	mm^{-3}	221.8	221.8	221.8	221.8	221.8
γ_0	mm^{-3}	110.9	110.9	110.9	110.9	110.9
aluminium foam						
γ_3	mm^{-3}	0.0116	0.0118	0.0129	0.0138	0.0137
V_3	mm^3	86.2	84.9	77.3	72.4	73.2
S_3	mm^2	114	110	97	85	93
B_3	mm	6.44	6.29	5.79	5.28	5.60
γ_2	mm^{-3}	0.0901	0.0903	0.0915	0.0923	0.0922
A_2	mm^2	7.3	7.2	6.9	6.4	6.9
γ_1	mm^{-3}	0.1571	0.1571	0.1571	0.1571	0.1571
γ_0	mm^{-3}	0.0785	0.0785	0.0785	0.0785	0.0785
nickel-chrome foam						
γ_3	mm^{-3}	8.62	8.75	9.61	10.26	10.15
V_3	mm^3	0.116	0.114	0.104	0.097	0.099
S_3	mm^2	1.384	1.343	1.188	1.039	1.130
B_3	mm	0.711	0.695	0.639	0.583	0.618
γ_2	mm^{-3}	66.97	67.10	67.96	68.61	68.50
A_2	mm^2	0.089	0.0876	0.0840	0.0777	0.0837
γ_1	mm^{-3}	116.7	116.7	116.7	116.7	116.7
γ_0	mm^{-3}	58.35	58.35	58.35	58.35	58.35

Table 4: Selected open foam features, measured under several model assumptions for the open nickel foam and the open aluminium foam. Measurements are based on χ_V.

5 Distribution of cell characteristics

5.1 Image analytic cell reconstruction

In order to measure characteristics of individual cells in an open foam, the pore space has to be divided into cells such that the edges coincide with the struts of the open foam. This so-called cell reconstruction starts with a binarisation yielding the strut system, followed by the Euclidean distance transform on the pores. After filtering the inverted distance image to remove superfluous local minima, the watershed transform is applied. (Inverted means here that each pixel gets as new grey value the difference of the maximal grey value for the given image type and its old grey value.) Finally, masking with the pore system yields the reconstructed cells.

The steps in this processing chain are explained in the following sections 5.1.1, 5.1.2, 5.1.3 with particular emphasis on the crucial filtering step.

5.1.1 Euclidean distance transform

Distance transforms operate on binary images and usually assign to each background pixel the distance to the foreground.

[ST94] developed the prototype of efficient algorithms for exact Euclidean distance transforms in 3d using the fact that the problem is separable. First, by one forward and one backward scan, determine the nearest foreground pixel in each x-column. Then, propagate the distance information in each y-column. Finally, the z-columns are processed. This algorithm results in exact squared Euclidean distances and has complexity $\mathcal{O}(m^4)$ if m is the number of pixels in x-, y-, and z-direction.

After generalising several 2d algorithms to 3d and comparing them empirically, Cuisenaire suggests a hybrid [Cui99, Section 6.4], performing particularly well on very large images, where it has a nearly linear complexity: First, on the x-y-slices, approximate distances are obtained by propagating the vector to the nearest foreground pixel within 4-pixel-neighbourhoods (a signed version of the four-point sequential distance mapping from [Dan80]). Subsequently, the approximate distance values are corrected by detecting the corners of the Voronoi tessellation generated by the foreground pixels, see [Cui99, Chapter 5]. Finally, the algorithm by [ST94] is applied for each column in z-direction.

5.1.2 Watershed transform

The watershed transform assigns a connected region to each local minimum in a grey value image. The transform can be interpreted as the flooding of a topographic surface, where the height is given by the grey value of the corresponding pixel: All local minima are water sources. The water rises uniformly with growing grey value. Pixels where waters from different sources meet are watershed pixels. The corresponding immersion algorithm of [VS91] can be easily extended to 3d and adapted to arbitrary adjacency systems.

Application of the watershed transform is hampered by the over-segmentation caused by the fact that *each* local minimum is assigned an image region. Strategies for overcoming this problem are pre-processing, modification, and post-processing. However, in the present application scenario the parameters for post-

processing like merging of basins are hard to deduce from the data. Therefore, we restrict ourselves to pre-processing and modification.

A modification with straightforward interpretation is the volume constrained pre-flooded watershed, where regions with volume below the threshold are merged with neighbour regions during immersion [TDK05]. Denote by t the volume threshold. In terms of the flooding analogy, the algorithm is altered in the following way: In each immersion step it is checked for the newly emerging basins whether their water surface is larger than t. (Note that this is a water surface in 4d corresponding to the volume of the catchment basin in 3d.) If this condition is met, immersion continues as in the unconstrained watershed algorithm. Otherwise, the pixels belonging to the basin are sent back to the queue of yet untreated pixels. If the basin size never reaches t, then finally water from a neighbouring basin spills over and thus the two regions are merged. This procedure is equivalent to an algebraic opening using all structuring elements with a volume smaller than t, see [Soi99, Section 4.4.2] for the 2d case, followed by the unconstrained watershed transform.

Generalisations to other sets of constraints like relative or absolute height of the minimum (contrast or brightness) are possible.

5.1.3 h-minima transform

Both the h-minima and the height adaptive h-minima transform are so called geodesic morphological transforms operating on two input images, typically the original one and a morphologically transformed version of it. For an overview over geodesic morphological transforms see [Soi99, Chapter 6].

The h-minima transform removes local grey value minima depending on their *dynamic*. In order to explain the idea of this transform, interpret the grey values as heights in a topological relief with bright pixels corresponding to mountain tops and dark pixels corresponding to valleys. The dynamic of a local minimum is the minimal height (number of grey levels) one has to overcome in order to reach a lower local grey value minimum. The local minima with dynamic lower than the parameter h are removed by filling 'valleys' in the grey value relief until either the local minimum is increased by h or water would spill into a valley of dynamic higher than h.

For a more precise description we have to introduce some notation: Let $\mathbb{F}$ be the adjacency system used for the foreground, $o = (0, 0, 0)$ the origin and write $\overline{xo}$ for the line segment connecting the points x and o. Denote by $N = \{x \in \mathbb{L}^3 \cap W : \overline{xo} \in \mathbb{F}\}$ the elementary neighbourhood given by the adjacency system $\mathbb{F}$.

The h-minima transform is a special case of reconstruction by erosion, which performs successive morphological erosions on a so called marker image restricted by a second image – the mask image.

Let f be the marker image and g the mask image. The grey values of the mask image have to be pixel-wise lower than those of the marker image $f \geq g$.

The marker image is eroded stepwise with N as structuring element. For a grey value image that means application of a minimum filter with filter mask N:

$$\mathscr{E}(f, N)(x) = \inf\{f(x + y) : y \in N\} \quad x \in \mathbb{L}^3 \cap W.$$

After each erosion step, the pixel-wise maximum of mask image g and eroded

marker image f_N is taken:

$$\mathscr{E}_g(f,N) = \mathscr{E}_g^{(1)}(f,N) = \max(\mathscr{E}(f,N), g).$$

We write

$$\mathscr{E}_g^{(i)}(f,N) = \mathscr{E}_g(\mathscr{E}_g^{(i-1)}(f,N), N)$$

for the i-th iteration of the geodesic erosion w. r. t. g. Due to the restriction given by g, there is a step (i) where another geodesic erosion step does not modify the image any further. The result is called reconstruction by erosion of f restricted by g:

$$\mathrm{rec}_g(f) := \mathscr{E}_g^{(i)}(f,N) \quad \text{where } i \text{ such that} \quad \mathscr{E}_g^{(i)}(f,N) = \mathscr{E}_g^{(i+1)}(f,N).$$

The h-minima transform is reconstruction by erosion with the original image serving as the marker image and $f + h$ as mask image

$$\mathrm{hmin}_h(f) := \mathrm{rec}_f(f + h).$$

For structures with strongly varying pore or cell sizes the parameter h can not be chosen such that non-relevant local minima in large cells disappear without removing local minima corresponding to centres of small cells. This problem can be overcome by adapting the parameter h to the total grey value, see [GS06]. After inversion of the distance image, centres of small pores correspond to local minima at a high absolute grey value. Centres of large pores are given by local minima at low absolute grey values. Thus the filtering should be strong at low grey values and very cautious at high grey values. Choosing $h = h(f(x))$ as a linearly decreasing function of the grey value fulfils these requirements. See Figure 6 for a sketch .

5.1.4 Complete reconstruction procedure

To summarise, the reconstruction procedure consists of

1. binarisation yielding the strut system
2. the Euclidean distance transform on the pores
3. inversion of the distance image (each pixel gets as new grey value the difference of the maximal grey value for the given image type and its old grey value)
4. optional:
   - filtering using the (adaptive) h-minima transform
   - reduce grey values of pixels in the pore system by 1
   - set grey values of pixels in the strut system to the maximum
5. either the watershed transform on the filtered image or the pre-flooded watershed transform on the filtered inverted distance image (result of step 4)
6. mask with the pore system

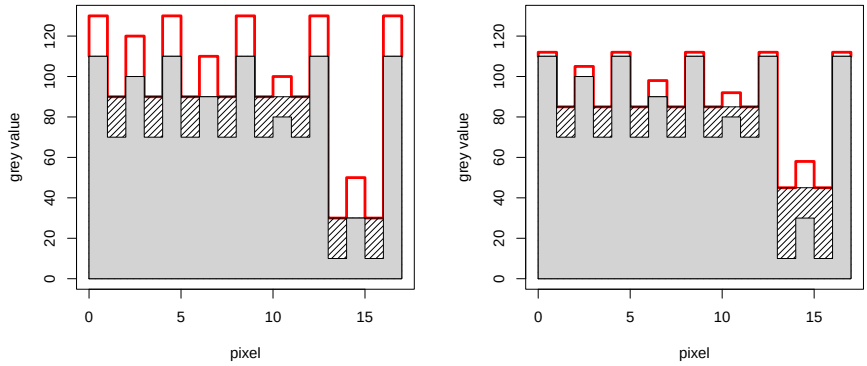

Figure 6: H-minima (left) and height adaptive h-minima transforms (right) on a 1d example. Grey: original image. Red: grey values increased by $h = 20$ or $h(f) = 38 - (f/3)$, respectively. Shaded: difference between original image and result. $h = 20$ unites the local minima of dynamic 10 and 20 both at high and low grey values (left). The adaptive transform filters the minima of dynamic 20 at low absolute grey value while conserving the high grey value minima of dynamic 20 (right).

The tedious steps in this processing chain are the decision between h-minima transform and pre-flooded watershed transform as well as the choice of the parameters for them.

The parameters for the pre-flooding or the h-minima transform can be deduced from the mean characteristics described in Section 4. More precisely, the pre-flooding parameter is closely connected to the mean cell volume whereas the parameter for the h-minima transform depends on the mean mean cell width.

Modification of the watershed algorithm is cheaper than pre-processing using grey value morphology in terms of both memory and time. However, results are difficult to compare as the h-minima transforms work globally on the image while the constraints during immersion only have local effects.

See Figure 7 for the cell reconstruction of the nickel-chrome foam from Figure 5 illustrated using 2d slices.

In order to give recommendations for both choice of the algorithm as well as choice of the parameters, a study using simulated data was performed. Methodology and results are presented in Section 5.3.

5.2 Characteristics of cells

The reconstructed cells are characterised by the intrinsic volumes (Section 2) as well as their diameters in the 13 discrete directions given by the axes, face diagonals and space diagonals of the unit cell of the lattice. (This set of geometric characteristics forms the ObjectFeatures in MAVI.)

Clearly for cells touching the boundary of the image, the features can not be determined correctly. Removing all boundary cells from the analysis induces a bias since large cells run a much higher risk to be hit by the boundary. Weighting

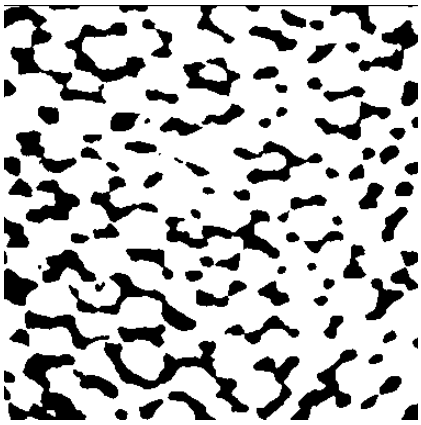

(a) Binary image of the strut system

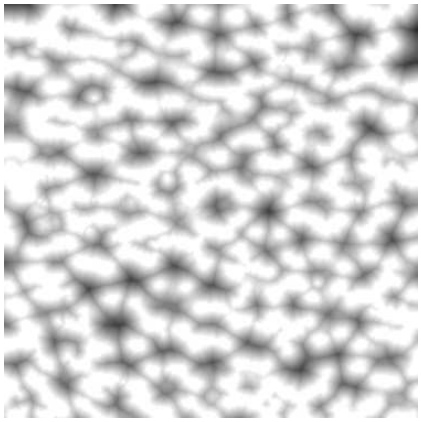

(b) Euclidean distance transform on pore space

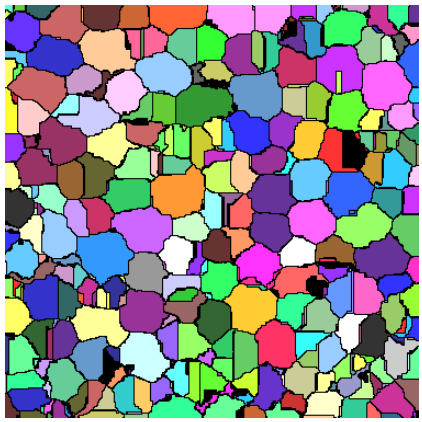

(c) Reconstruction without pre-processing

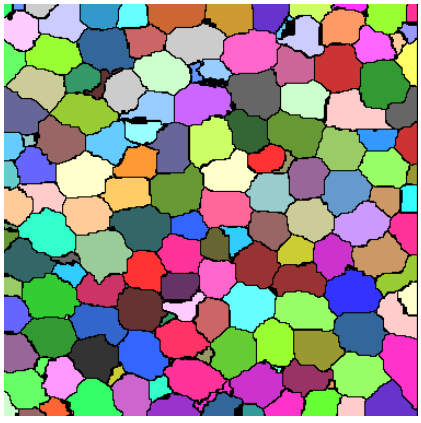

(d) Smoothed with h-minima transform, $h = 0.5B_3$

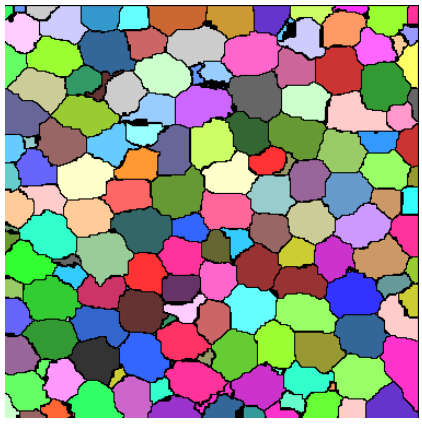

(e) Smoothed with pre-flooded watershed transform, $t = 0.4V_3$

Figure 7: Influence of different pre-processing to the pore reconstruction, illustrated using 2d slices of the nickel-chrome foam (see Figure 5). Both hmin transform and pre-flooded watershed yield good results, differences between the reconstruction results are small and mostly located near the image edges.

with the reciprocal of the probability of being observed (Horvitz Thompson procedure, see [Bad99, 2.4]) is one way to correct for this bias. In our context, that means weighting with the fraction of volume of the whole sample and volume of the sample reduced by the bounding box of the cell (Miles Lantuejoul correction, see [Ser82, pp. 246]). If the sample is large enough, minus sampling is an alternative: Reduce the observation window such that all cells with centre of the bounding box inside this sub-window are contained completely in the original observation window.

For the nickel-chrome foam, the histograms of the cell volumes obtained using both edge corrections are shown in Figure 8. The estimated mean cell sizes (0.0735mm^3 and 0.0745mm^3) differ only slightly but they are significantly lower than the corresponding values obtained directly from the strut system (Table 4). The cell reconstruction process bears two sources of underestimation of V_3 – over-segmentation by the watershed algorithm and missing large cells due to edge effects. However, in view of the estimation results reported in Table 3, overestimation of V_3 when using the strut system is the most plausible explanation: In the nickel-chrome foam, the strut diameter is larger than 20 pixels. Thus the scaling factor is overestimated by at least 1.13 resulting in an overestimation of V_3 by 1.44 and $1.44 \cdot 0.074 = 0.107$.

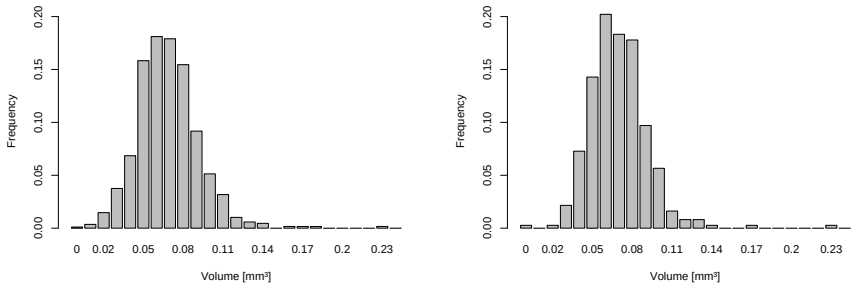

(a) Edge correction by weighting, $V_3 = 0.0735\text{mm}^3$

(b) Minus sampling, $V_3 = 0.0745\text{mm}^3$

Figure 8: Empirical distribution of the cell volume for the nickel-chrome foam. Cells reconstructed using the pre-flooded watershed transform with $t = 0.4\,V_3$.

A slightly different estimation procedure is used when estimating cell characteristics for comparison with simulated data only. Realizations of tessellation models consist of space filling polyhedra without additional dividing walls. Therefore, instead of the final masking with the pore system, we rather dilate the pores by the unit cell of the lattice in order to remove all watersheds.

5.3 Choice of algorithm and parameters in the reconstruction process

The reconstruction procedure described in Section 5.1.4 was applied to the edge systems of random Laguerre tessellations generated by force biased packings of approximately 4 500 balls with gamma distributed size and $V_V = 0.6$. Subsequently, the cells in the original data set and in the reconstructed one were matched using the centre of the bounding box as landmark. For the evaluation of

the reconstruction algorithm, only cells not touching the border in both images were taken into account. This results in approximately 2 600 cells considered.

As could be expected, the quality of the reconstruction depends on the variability of the cell sizes. However, the parameters for both the h-minima and the pre-flooded watershed transform can be chosen very small as the simulated data are free of all sources of superfluous maxima in the distance image other than discretisation effects. The best results are obtained for parameters in the range $[0.5\%B_3, 1\%B_3]$ for the h-minima transform and $[0.003\%V_3, 0.02\%V_3]$ for the pre-flooded watershed transform.

For coefficients of variation in the range $[0.4, 1.2]$ less than 0.5% of the cells are wrongly reconstructed. The mean deviation in the volume measurement is smaller than 5%. For $cv = 1.4$ the fraction of wrongly reconstructed cells is still just 1.7% and the mean volume deviation 6.32%.

In all cases the results for the optimal parameters for both pre-flooded watershed and hmin transform are very close. Reconstruction using the pre-flooded watershed seems to be more robust w. r. t. deviation from the optimal parameter. The results prove that the reconstruction method yields correct results, also for ranges of cell size variation typically observed in real solid foams. However, the parameters found to be optimal for the simulated data are far from those used for real data. Thus no recommendations for the choice of parameters for real foam data can be deduced. This needs another simulation study incorporating the sources for over-segmentation found in real data: noise, distortion, surface roughness.

For strongly varying cell sizes ($cv = 2.0$), the cell reconstruction process fails: Choosing $h = 1\%B_3$ results in 130 out of 2 682 cells disappearing while still 20 are over-segmented, that is cut into two. In both cases, medium size cells close to large ones are effected as their shape is far from spheroidal. Therefore also the h-minima transform adapted linearly, logarithmically, and as square-root to the grey values does not yield better results. Nevertheless, the adaptive h-minima transform can still yield proper reconstruction results where the other methods fail as in the following example (see Figure 9). However, the choice of the adaption function as well as the parameters remains time consuming as it is done by trial-and-error.

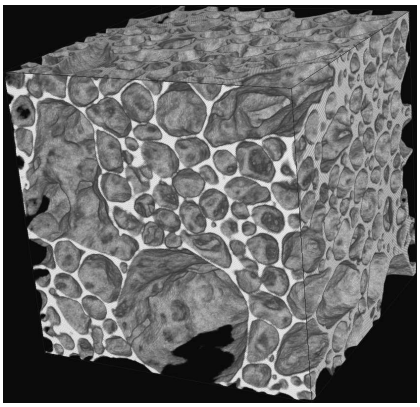

(a) volume rendering

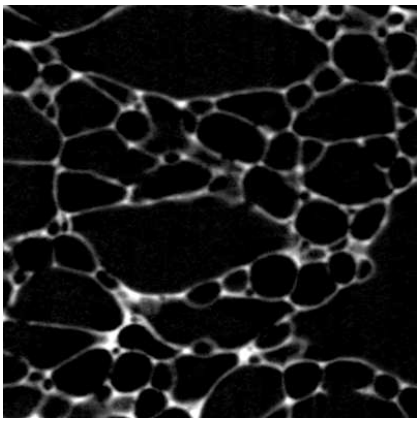

(b) original slice

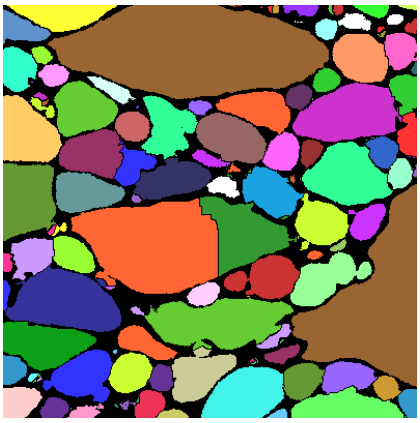

(c) hmin

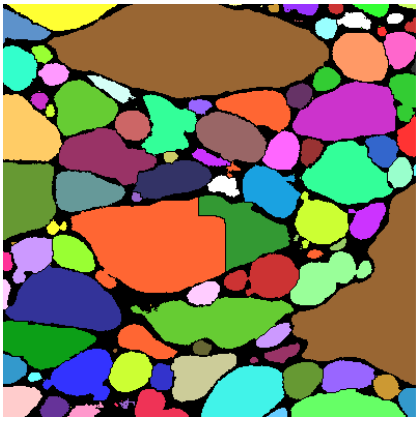

(d) pre-flooded watershed

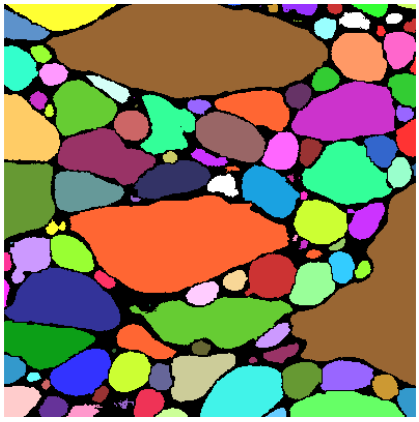

(e) linearly adaptive hmin

Figure 9: Closed cell aluminium foam, $400 \times 400 \times 400$ pixels, pixel size 40μm, corresponding to $16 \times 16 \times 16\text{mm}^3$. μCT imaging by BAM, sample from TU Freiberg. Cell reconstruction results. Both hmin and pre-flooded watershed already over-smooth some of the small cells while the large one in the centre of the shown slice is wrongly cut into two. Thus different parameters would not improve the reconstruction result significantly. The height adaptive hmin transform overcomes this problem.

6 Discussion

The simulation study in Section 4 shows a clear advantage of estimating the mean values of cell characteristics of open foams based on the Euler number density of the strut system χ_V instead of the specific strut length L_V. Moreover, it indicates that the estimation could be improved by changing the correction factor for L_V and finding a suitable correction for χ_V. Further simulation studies with data closer to μCT images of real solid foams have to be performed to verify the monotone increase of the bias with the strut thickness.

Estimation of foam characteristics without cell reconstruction is very attractive as it is a magnitude faster and much less error prone. However, only mean values can be achieved that way. These are not sufficient for characterisation of the foam structure, in particular when fitting a geometric model is the final goal, see [Lau08]. Therefore simple and possibly rough estimates for second moments of cell characteristics have to be found either for direct use or as input for an automatic reconstruction procedure.

The optimal reconstruction parameters obtained by the simulation study in Section 5.3 are far from those usually used for real foams. The edge systems of Laguerre tessellations generated by close ball packings are good models for open foams. Nevertheless, the major sources for superfluous local maxima in the distance image causing over-segmentation by the watershed transform are neither discretisation effects nor deviation from ball shape caused by a uniform scaling of all cells. Thus the models have to be supplemented by bent or tilted struts or cells and surface roughness, in order to achieve recommendations for the choice of parameters for real foams.

So far, the reconstruction results for real data are evaluated essentially visually. Automatic detection of over- or under-segmentation seems out of reach. However, visual inspection could be supported e. g. by finding suspicious reconstructed cells based on their shape or shape and direction of the watersheds.

Acknowledgement

We thank Christina Stöhr for experiments and programming and Helga Riedel for the 3d visualisations. The work on this report was partially funded by the project "Virtual material design" within BMBF project 01 SF 0708 (Fraunhofer-Carnot Cooperation).

References

[Aur87] F. Aurenhammer. A Criterion for the Affine Equivalence of Cell Complexes in $\mathbb{R}^d$ and Convex Polyhedra in $\mathbb{R}^{d+1}$. *Discrete & Computational Geometry*, 2:49–64, 1987.

[Bad99] A. J. Baddeley. Spatial sampling and censoring. In W.S. Kendall, M.N.M. van Lieshout, and O.E. Barndorff-Nielsen, editors, *Stochastic Geometry: Likelihood and Computation*. Chapman and Hall, London, 1999.

[BBS02] A. Bezrukov, M. Bargieł, and D. Stoyan. Statistical analysis of simulated random packings of spheres. *Part. Part. Systems Char.*, 19:111–118, 2002.

[Cui99] O. Cuisenaire. *Distance transformations: fast algorithms and applications to medical image processing.* PhD thesis, Université catholique de Louvain, Louvain, 1999. `http://www.tele.ucl.ac.be/PEOPLE/OC/these.pdf`.

[Dan80] P. E. Danielsson. Euclidean distance mapping. *Computer Vision, Graphics, and Image Processing*, 14:227–248, 1980.

[Fra05] Fraunhofer ITWM, Department of Image Processing. MAVI – modular algorithms for volume images. `http://www.itwm.fhg.de/mab/projects/MAVI/`, 2005.

[FWZL04] Z. Fan, Y. Wu, X. Zhao, and Y. Lu. Simulation of polycrystalline structure with Voronoi diagram in Laguerre geometry based on random closed packing of spheres. *Computational Materials Science*, 29:301–308, 2004.

[GS06] M. Godehardt and K. Schladitz. Geometric characterisation of light weight composites using computer tomographic images. In *Proceedings of the 9th European NDT Conference*, Berlin, 2006.

[JJCL04] J. P. Jernot, P. Jouannot-Chesney, and C. Lantuéjoul. Local contributions to the Euler-Poincaré characteristic of a set. *J. Microsc.*, 215:40–49, 2004.

[Lau07] C. Lautensack. *Random Laguerre Tessellations.* PhD thesis, Universität Karlsruhe, Verlag Lautensack, Weiler bei Bingen, 2007.

[Lau08] C. Lautensack. Fitting three-dimensional Laguerre tessellations to foam structures. *Journal of Applied Statistics*, 35(9):985–995, 2008.

[LH93] U. Lorz and U. Hahn. Geometric characteristics of spatial voronoi tessellations and planar sections. Technical Report 93-05, Fachbereich Mathematik,TU Bergakademie Freiberg, 1993.

[LS06] C. Lautensack and T. Sych. 3d image analysis of open foams using random tessellations. *Image Analysis and Stereology*, 25:87–93, 2006.

[LS08] C. Lautensack and T. Sych. A random Weaire-Phelan foam. In *8th International Conference on Stereology and Image Analysis in Materials Science STERMAT 2008*, Zakopane, Poland, September 2008.

[LZ08] C. Lautensack and S. Zuyev. Random Laguerre tessellations. *Advances in Applied Probability*, 40(3), 2008. to appear.

[Mec80] J. Mecke. Palm methods for stationary random mosaics. In *Combinatorial principles in stochastic geometry, Work Collect.*, pages 124–132. Erevan, 1980.

[OM00] J. Ohser and F. Mücklich. *Statistical Analysis of Microstructures in Materials Science*. J. Wiley & Sons, Chichester, New York, 2000.

[OS08] J. Ohser and K. Schladitz. Visualisation, processing and analysis of tomographic data. In J. Banhart, editor, *Advanced Tomographic Methods in Materials Research and Engineering*. Oxford University Press, 2008.

[Red08] C. Redenbach. Microstructure models for cellular materials. *Computational Materials Science*, 2008. accepted.

[Sch93] R. Schneider. *Convex Bodies. The Brunn–Minkowski Theory*. Cambridge University Press, Cambridge, 1993.

[Ser82] J. Serra. *Image Analysis and Mathematical Morphology, volume 1*. Academic Press, London, 1982.

[SKM95] D. Stoyan, W. S. Kendall, and J. Mecke. *Stochastic Geometry and Its Applications*. Wiley, Chichester, 2nd edition, 1995.

[Soi99] P. Soille. *Morphological Image Analysis*. Springer, Berlin, 1999.

[SON06] K. Schladitz, J. Ohser, and W. Nagel. Measurement of intrinsic volumes of sets observed on lattices. In A. Kuba, L. G. Nyul, and K. Palagyi, editors, *13th International Conference on Discrete Geometry for Computer Imagery*, volume 4245 of *LNCS*, pages 247–258, Berlin, Heidelberg, New York, October 2006. DGCI, Szeged, Hungary, Springer.

[ST94] T. Saito and J. Toriwaki. New algorithms for euclidean distance transformations of an n-dimensional digitised picture with applications. *Pattern Recognition*, 27(11):1551–1565, 1994.

[SW08] R. Schneider and W. Weil. *Stochastic and Integral Geometry*. Springer, Berlin, Heidelberg, New York, 2008.

[Syc04] T. Sych. Estimation of geometric characteristics of foam structures. Master's thesis, Universität Kaiserslautern/Fraunhofer ITWM, Kaiserslautern, 2004.

[TDK05] F. B. Tek, A. G. Dempster, and I. Kale. Blood cell segmentation using minimum area watershed and circle Radon transformations. In C. Ronse, L. Najman, and E. Decencire, editors, *Proc. Int. Symp. on Mathematical Morphology*, volume 30 of *Computational Imaging and Vision*, pages 441–454, Dordrecht, April 2005. Springer.

[VS91] L. Vincent and P. Soille. Watersheds in digital spaces: An efficient algorithm based on immersion simulation. *IEEE Transactions on Pattern Analysis and Machine Intelligence*, 13(6):583–598, 1991.

[Wea96] D. Weaire, editor. *The Kelvin Problem: Foam Structures of Minimal Surface Area*. Taylor & Francis, London, 1996.

Published reports of the Fraunhofer ITWM

The PDF-files of the following reports are available under:
www.itwm.fraunhofer.de/de/zentral__berichte/berichte

1. D. Hietel, K. Steiner, J. Struckmeier
A Finite - Volume Particle Method for Compressible Flows
(19 pages, 1998)

2. M. Feldmann, S. Seibold
Damage Diagnosis of Rotors: Application of Hilbert Transform and Multi-Hypothesis Testing
Keywords: Hilbert transform, damage diagnosis, Kalman filtering, non-linear dynamics
(23 pages, 1998)

3. Y. Ben-Haim, S. Seibold
Robust Reliability of Diagnostic Multi-Hypothesis Algorithms: Application to Rotating Machinery
Keywords: Robust reliability, convex models, Kalman filtering, multi-hypothesis diagnosis, rotating machinery, crack diagnosis
(24 pages, 1998)

4. F.-Th. Lentes, N. Siedow
Three-dimensional Radiative Heat Transfer in Glass Cooling Processes
(23 pages, 1998)

5. A. Klar, R. Wegener
A hierarchy of models for multilane vehicular traffic
Part I: Modeling
(23 pages, 1998)

Part II: Numerical and stochastic investigations
(17 pages, 1998)

6. A. Klar, N. Siedow
Boundary Layers and Domain Decomposition for Radiative Heat Transfer and Diffusion Equations: Applications to Glass Manufacturing Processes
(24 pages, 1998)

7. I. Choquet
Heterogeneous catalysis modelling and numerical simulation in rarified gas flows Part I: Coverage locally at equilibrium
(24 pages, 1998)

8. J. Ohser, B. Steinbach, C. Lang
Efficient Texture Analysis of Binary Images
(17 pages, 1998)

9. J. Orlik
Homogenization for viscoelasticity of the integral type with aging and shrinkage
(20 pages, 1998)

10. J. Mohring
Helmholtz Resonators with Large Aperture
(21 pages, 1998)

11. H. W. Hamacher, A. Schöbel
On Center Cycles in Grid Graphs
(15 pages, 1998)

12. H. W. Hamacher, K.-H. Küfer
Inverse radiation therapy planning - a multiple objective optimisation approach
(14 pages, 1999)

13. C. Lang, J. Ohser, R. Hilfer
On the Analysis of Spatial Binary Images
(20 pages, 1999)

14. M. Junk
On the Construction of Discrete Equilibrium Distributions for Kinetic Schemes
(24 pages, 1999)

15. M. Junk, S. V. Raghurame Rao
A new discrete velocity method for Navier-Stokes equations
(20 pages, 1999)

16. H. Neunzert
Mathematics as a Key to Key Technologies
(39 pages (4 PDF-Files), 1999)

17. J. Ohser, K. Sandau
Considerations about the Estimation of the Size Distribution in Wicksell's Corpuscle Problem
(18 pages, 1999)

18. E. Carrizosa, H. W. Hamacher, R. Klein, S. Nickel
Solving nonconvex planar location problems by finite dominating sets
Keywords: Continuous Location, Polyhedral Gauges, Finite Dominating Sets, Approximation, Sandwich Algorithm, Greedy Algorithm
(19 pages, 2000)

19. A. Becker
A Review on Image Distortion Measures
Keywords: Distortion measure, human visual system
(26 pages, 2000)

20. H. W. Hamacher, M. Labbé, S. Nickel, T. Sonneborn
Polyhedral Properties of the Uncapacitated Multiple Allocation Hub Location Problem
Keywords: integer programming, hub location, facility location, valid inequalities, facets, branch and cut
(21 pages, 2000)

21. H. W. Hamacher, A. Schöbel
Design of Zone Tariff Systems in Public Transportation
(30 pages, 2001)

22. D. Hietel, M. Junk, R. Keck, D. Teleaga
The Finite-Volume-Particle Method for Conservation Laws
(16 pages, 2001)

23. T. Bender, H. Hennes, J. Kalcsics, M. T. Melo, S. Nickel
Location Software and Interface with GIS and Supply Chain Management
Keywords: facility location, software development, geographical information systems, supply chain management
(48 pages, 2001)

24. H. W. Hamacher, S. A. Tjandra
Mathematical Modelling of Evacuation Problems: A State of Art
(44 pages, 2001)

25. J. Kuhnert, S. Tiwari
Grid free method for solving the Poisson equation
Keywords: Poisson equation, Least squares method, Grid free method
(19 pages, 2001)

26. T. Götz, H. Rave, D. Reinel-Bitzer, K. Steiner, H. Tiemeier
Simulation of the fiber spinning process
Keywords: Melt spinning, fiber model, Lattice Boltzmann, CFD
(19 pages, 2001)

27. A. Zemitis
On interaction of a liquid film with an obstacle
Keywords: impinging jets, liquid film, models, numerical solution, shape
(22 pages, 2001)

28. I. Ginzburg, K. Steiner
Free surface lattice-Boltzmann method to model the filling of expanding cavities by Bingham Fluids
Keywords: Generalized LBE, free-surface phenomena, interface boundary conditions, filling processes, Bingham viscoplastic model, regularized models
(22 pages, 2001)

29. H. Neunzert
»Denn nichts ist für den Menschen als Menschen etwas wert, was er nicht mit Leidenschaft tun kann«
Vortrag anlässlich der Verleihung des Akademiepreises des Landes Rheinland-Pfalz am 21.11.2001
Keywords: Lehre, Forschung, angewandte Mathematik, Mehrskalenanalyse, Strömungsmechanik
(18 pages, 2001)

30. J. Kuhnert, S. Tiwari
Finite pointset method based on the projection method for simulations of the incompressible Navier-Stokes equations
Keywords: Incompressible Navier-Stokes equations, Meshfree method, Projection method, Particle scheme, Least squares approximation
AMS subject classification: 76D05, 76M28
(25 pages, 2001)

31. R. Korn, M. Krekel
Optimal Portfolios with Fixed Consumption or Income Streams
Keywords: Portfolio optimisation, stochastic control, HJB equation, discretisation of control problems
(23 pages, 2002)

32. M. Krekel
Optimal portfolios with a loan dependent credit spread
Keywords: Portfolio optimisation, stochastic control, HJB equation, credit spread, log utility, power utility, non-linear wealth dynamics
(25 pages, 2002)

33. J. Ohser, W. Nagel, K. Schladitz
The Euler number of discretized sets – on the choice of adjacency in homogeneous lattices
Keywords: image analysis, Euler number, neighborhod relationships, cuboidal lattice
(32 pages, 2002)

34. I. Ginzburg, K. Steiner
Lattice Boltzmann Model for Free-Surface flow and Its Application to Filling Process in Casting
Keywords: Lattice Boltzmann models; free-surface phenomena; interface boundary conditions; filling processes; injection molding; volume of fluid method; interface boundary conditions; advection-schemes; upwind-schemes
(54 pages, 2002)

35. M. Günther, A. Klar, T. Materne, R. Wegener
Multivalued fundamental diagrams and stop and go waves for continuum traffic equations
Keywords: traffic flow, macroscopic equations, kinetic derivation, multivalued fundamental diagram, stop and go waves, phase transitions
(25 pages, 2002)

36. S. Feldmann, P. Lang, D. Prätzel-Wolters
Parameter influence on the zeros of network determinants
Keywords: Networks, Equicofactor matrix polynomials, Realization theory, Matrix perturbation theory
(30 pages, 2002)

37. K. Koch, J. Ohser, K. Schladitz
Spectral theory for random closed sets and estimating the covariance via frequency space
Keywords: Random set, Bartlett spectrum, fast Fourier transform, power spectrum
(28 pages, 2002)

38. D. d'Humières, I. Ginzburg
Multi-reflection boundary conditions for lattice Boltzmann models
Keywords: lattice Boltzmann equation, boudary condistions, bounce-back rule, Navier-Stokes equation
(72 pages, 2002)

39. R. Korn
Elementare Finanzmathematik
Keywords: Finanzmathematik, Aktien, Optionen, Portfolio-Optimierung, Börse, Lehrerweiterbildung, Mathematikunterricht
(98 pages, 2002)

40. J. Kallrath, M. C. Müller, S. Nickel
Batch Presorting Problems: Models and Complexity Results
Keywords: Complexity theory, Integer programming, Assigment, Logistics
(19 pages, 2002)

41. J. Linn
On the frame-invariant description of the phase space of the Folgar-Tucker equation
Key words: fiber orientation, Folgar-Tucker equation, injection molding
(5 pages, 2003)

42. T. Hanne, S. Nickel
A Multi-Objective Evolutionary Algorithm for Scheduling and Inspection Planning in Software Development Projects
Key words: multiple objective programming, project management and scheduling, software development, evolutionary algorithms, efficient set
(29 pages, 2003)

43. T. Bortfeld , K.-H. Küfer, M. Monz, A. Scherrer, C. Thieke, H. Trinkaus
Intensity-Modulated Radiotherapy - A Large Scale Multi-Criteria Programming Problem
Keywords: multiple criteria optimization, representative systems of Pareto solutions, adaptive triangulation, clustering and disaggregation techniques, visualization of Pareto solutions, medical physics, external beam radiotherapy planning, intensity modulated radiotherapy
(31 pages, 2003)

44. T. Halfmann, T. Wichmann
Overview of Symbolic Methods in Industrial Analog Circuit Design
Keywords: CAD, automated analog circuit design, symbolic analysis, computer algebra, behavioral modeling, system simulation, circuit sizing, macro modeling, differential-algebraic equations, index
(17 pages, 2003)

45. S. E. Mikhailov, J. Orlik
Asymptotic Homogenisation in Strength and Fatigue Durability Analysis of Composites
Keywords: multiscale structures, asymptotic homogenization, strength, fatigue, singularity, non-local conditions
(14 pages, 2003)

46. P. Domínguez-Marín, P. Hansen, N. Mladenovi´c , S. Nickel
Heuristic Procedures for Solving the Discrete Ordered Median Problem
Keywords: genetic algorithms, variable neighborhood search, discrete facility location
(31 pages, 2003)

47. N. Boland, P. Domínguez-Marín, S. Nickel, J. Puerto
Exact Procedures for Solving the Discrete Ordered Median Problem
Keywords: discrete location, Integer programming
(41 pages, 2003)

48. S. Feldmann, P. Lang
Padé-like reduction of stable discrete linear systems preserving their stability
Keywords: Discrete linear systems, model reduction, stability, Hankel matrix, Stein equation
(16 pages, 2003)

49. J. Kallrath, S. Nickel
A Polynomial Case of the Batch Presorting Problem
Keywords: batch presorting problem, online optimization, competetive analysis, polynomial algorithms, logistics
(17 pages, 2003)

50. T. Hanne, H. L. Trinkaus
knowCube for MCDM – Visual and Interactive Support for Multicriteria Decision Making
Key words: Multicriteria decision making, knowledge management, decision support systems, visual interfaces, interactive navigation, real-life applications.
(26 pages, 2003)

51. O. Iliev, V. Laptev
On Numerical Simulation of Flow Through Oil Filters
Keywords: oil filters, coupled flow in plain and porous media, Navier-Stokes, Brinkman, numerical simulation
(8 pages, 2003)

52. W. Dörfler, O. Iliev, D. Stoyanov, D. Vassileva
On a Multigrid Adaptive Refinement Solver for Saturated Non-Newtonian Flow in Porous Media
Keywords: Nonlinear multigrid, adaptive refinement, non-Newtonian flow in porous media
(17 pages, 2003)

53. S. Kruse
On the Pricing of Forward Starting Options under Stochastic Volatility
Keywords: Option pricing, forward starting options, Heston model, stochastic volatility, cliquet options
(11 pages, 2003)

54. O. Iliev, D. Stoyanov
Multigrid – adaptive local refinement solver for incompressible flows
Keywords: Navier-Stokes equations, incompressible flow, projection-type splitting, SIMPLE, multigrid methods, adaptive local refinement, lid-driven flow in a cavity
(37 pages, 2003)

55. V. Starikovicius
The multiphase flow and heat transfer in porous media
Keywords: Two-phase flow in porous media, various formulations, global pressure, multiphase mixture model, numerical simulation
(30 pages, 2003)

56. P. Lang, A. Sarishvili, A. Wirsen
Blocked neural networks for knowledge extraction in the software development process
Keywords: Blocked Neural Networks, Nonlinear Regression, Knowledge Extraction, Code Inspection
(21 pages, 2003)

57. H. Knaf, P. Lang, S. Zeiser
Diagnosis aiding in Regulation Thermography using Fuzzy Logic
Keywords: fuzzy logic,knowledge representation, expert system
(22 pages, 2003)

58. M. T. Melo, S. Nickel, F. Saldanha da Gama
Largescale models for dynamic multicommodity capacitated facility location
Keywords: supply chain management, strategic planning, dynamic location, modeling
(40 pages, 2003)

59. J. Orlik
Homogenization for contact problems with periodically rough surfaces
Keywords: asymptotic homogenization, contact problems
(28 pages, 2004)

60. A. Scherrer, K.-H. Küfer, M. Monz, F. Alonso, T. Bortfeld
IMRT planning on adaptive volume structures – a significant advance of computational complexity
Keywords: Intensity-modulated radiation therapy (IMRT), inverse treatment planning, adaptive volume structures, hierarchical clustering, local refinement, adaptive clustering, convex programming, mesh generation, multi-grid methods
(24 pages, 2004)

61. D. Kehrwald
Parallel lattice Boltzmann simulation of complex flows
Keywords: Lattice Boltzmann methods, parallel computing, microstructure simulation, virtual material design, pseudo-plastic fluids, liquid composite moulding
(12 pages, 2004)

62. O. Iliev, J. Linn, M. Moog, D. Niedziela, V. Starikovicius
On the Performance of Certain Iterative Solvers for Coupled Systems Arising in Discretization of Non-Newtonian Flow Equations
Keywords: Performance of iterative solvers, Preconditioners, Non-Newtonian flow
(17 pages, 2004)

63. R. Ciegis, O. Iliev, S. Rief, K. Steiner
On Modelling and Simulation of Different Regimes for Liquid Polymer Moulding
Keywords: Liquid Polymer Moulding, Modelling, Simulation, Infiltration, Front Propagation, non-Newtonian flow in porous media
(43 pages, 2004)

64. T. Hanne, H. Neu
Simulating Human Resources in Software Development Processes
Keywords: Human resource modeling, software process, productivity, human factors, learning curve
(14 pages, 2004)

65. O. Iliev, A. Mikelic, P. Popov
Fluid structure interaction problems in deformable porous media: Toward permeability of deformable porous media
Keywords: fluid-structure interaction, deformable porous media, upscaling, linear elasticity, stokes, finite elements
(28 pages, 2004)

66. F. Gaspar, O. Iliev, F. Lisbona, A. Naumovich, P. Vabishchevich
On numerical solution of 1-D poroelasticity equations in a multilayered domain
Keywords: poroelasticity, multilayered material, finite volume discretization, MAC type grid
(41 pages, 2004)

67. J. Ohser, K. Schladitz, K. Koch, M. Nöthe
Diffraction by image processing and its application in materials science
Keywords: porous microstructure, image analysis, random set, fast Fourier transform, power spectrum, Bartlett spectrum
(13 pages, 2004)

68. H. Neunzert
Mathematics as a Technology: Challenges for the next 10 Years
Keywords: applied mathematics, technology, modelling, simulation, visualization, optimization, glass processing, spinning processes, fiber-fluid interaction, trubulence effects, topological optimization, multicriteria optimization, Uncertainty and Risk, financial mathematics, Malliavin calculus, Monte-Carlo methods, virtual material design, filtration, bio-informatics, system biology
(29 pages, 2004)

69. R. Ewing, O. Iliev, R. Lazarov, A. Naumovich
On convergence of certain finite difference discretizations for 1D poroelasticity interface problems
Keywords: poroelasticity, multilayered material, finite volume discretizations, MAC type grid, error estimates
(26 pages,2004)

70. W. Dörfler, O. Iliev, D. Stoyanov, D. Vassileva
On Efficient Simulation of Non-Newtonian Flow in Saturated Porous Media with a Multigrid Adaptive Refinement Solver
Keywords: Nonlinear multigrid, adaptive renement, non-Newtonian in porous media
(25 pages, 2004)

71. J. Kalcsics, S. Nickel, M. Schröder
Towards a Unified Territory Design Approach – Applications, Algorithms and GIS Integration
Keywords: territory desgin, political districting, sales territory alignment, optimization algorithms, Geographical Information Systems
(40 pages, 2005)

72. K. Schladitz, S. Peters, D. Reinel-Bitzer, A. Wiegmann, J. Ohser
Design of acoustic trim based on geometric modeling and flow simulation for non-woven
Keywords: random system of fibers, Poisson line process, flow resistivity, acoustic absorption, Lattice-Boltzmann method, non-woven
(21 pages, 2005)

73. V. Rutka, A. Wiegmann
Explicit Jump Immersed Interface Method for virtual material design of the effective elastic moduli of composite materials
Keywords: virtual material design, explicit jump immersed interface method, effective elastic moduli, composite materials
(22 pages, 2005)

74. T. Hanne
Eine Übersicht zum Scheduling von Baustellen
Keywords: Projektplanung, Scheduling, Bauplanung, Bauindustrie
(32 pages, 2005)

75. J. Linn
The Folgar-Tucker Model as a Differetial Algebraic System for Fiber Orientation Calculation
Keywords: fiber orientation, Folgar–Tucker model, invariants, algebraic constraints, phase space, trace stability
(15 pages, 2005)

76. M. Speckert, K. Dreßler, H. Mauch, A. Lion, G. J. Wierda
Simulation eines neuartigen Prüfsystems für Achserprobungen durch MKS-Modellierung einschließlich Regelung
Keywords: virtual test rig, suspension testing, multibody simulation, modeling hexapod test rig, optimization of test rig configuration
(20 pages, 2005)

77. K.-H. Küfer, M. Monz, A. Scherrer, P. Süss, F. Alonso, A. S. A. Sultan, Th. Bortfeld, D. Craft, Chr. Thieke
Multicriteria optimization in intensity modulated radiotherapy planning
Keywords: multicriteria optimization, extreme solutions, real-time decision making, adaptive approximation schemes, clustering methods, IMRT planning, reverse engineering
(51 pages, 2005)

78. S. Amstutz, H. Andrä
A new algorithm for topology optimization using a level-set method
Keywords: shape optimization, topology optimization, topological sensitivity, level-set
(22 pages, 2005)

79. N. Ettrich
Generation of surface elevation models for urban drainage simulation
Keywords: Flooding, simulation, urban elevation models, laser scanning
(22 pages, 2005)

80. H. Andrä, J. Linn, I. Matei, I. Shklyar, K. Steiner, E. Teichmann
OPTCAST – Entwicklung adäquater Strukturoptimierungsverfahren für Gießereien Technischer Bericht (KURZFASSUNG)
Keywords: Topologieoptimierung, Level-Set-Methode, Gießprozesssimulation, Gießtechnische Restriktionen, CAE-Kette zur Strukturoptimierung
(77 pages, 2005)

81. N. Marheineke, R. Wegener
Fiber Dynamics in Turbulent Flows Part I: General Modeling Framework
Keywords: fiber-fluid interaction; Cosserat rod; turbulence modeling; Kolmogorov's energy spectrum; double-velocity correlations; differentiable Gaussian fields
(20 pages, 2005)

Part II: Specific Taylor Drag
Keywords: flexible fibers; k-ε turbulence model; fiber-turbulence interaction scales; air drag; random Gaussian aerodynamic force; white noise; stochastic differential equations; ARMA process
(18 pages, 2005)

82. C. H. Lampert, O. Wirjadi
An Optimal Non-Orthogonal Separation of the Anisotropic Gaussian Convolution Filter
Keywords: Anisotropic Gaussian filter, linear filtering, orientation space, nD image processing, separable filters
(25 pages, 2005)

83. H. Andrä, D. Stoyanov
Error indicators in the parallel finite element solver for linear elasticity DDFEM
Keywords: linear elasticity, finite element method, hierarchical shape functions, domain decom-position, parallel implementation, a posteriori error estimates
(21 pages, 2006)

84. M. Schröder, I. Solchenbach
Optimization of Transfer Quality in Regional Public Transit
Keywords: public transit, transfer quality, quadratic assignment problem
(16 pages, 2006)

85. A. Naumovich, F. J. Gaspar
On a multigrid solver for the three-dimensional Biot poroelasticity system in multilayered domains
Keywords: poroelasticity, interface problem, multigrid, operator-dependent prolongation
(11 pages, 2006)

86. S. Panda, R. Wegener, N. Marheineke
Slender Body Theory for the Dynamics of Curved Viscous Fibers
Keywords: curved viscous fibers; fluid dynamics; Navier-Stokes equations; free boundary value problem; asymptotic expansions; slender body theory
(14 pages, 2006)

87. E. Ivanov, H. Andrä, A. Kudryavtsev
Domain Decomposition Approach for Automatic Parallel Generation of Tetrahedral Grids
Key words: Grid Generation, Unstructured Grid, Delaunay Triangulation, Parallel Programming, Domain Decomposition, Load Balancing
(18 pages, 2006)

88. S. Tiwari, S. Antonov, D. Hietel, J. Kuhnert, R. Wegener
A Meshfree Method for Simulations of Interactions between Fluids and Flexible Structures
Key words: Meshfree Method, FPM, Fluid Structure Interaction, Sheet of Paper, Dynamical Coupling
(16 pages, 2006)

89. R. Ciegis , O. Iliev, V. Starikovicius, K. Steiner
Numerical Algorithms for Solving Problems of Multiphase Flows in Porous Media
Keywords: nonlinear algorithms, finite-volume method, software tools, porous media, flows
(16 pages, 2006)

90. D. Niedziela, O. Iliev, A. Latz
On 3D Numerical Simulations of Viscoelastic Fluids
Keywords: non-Newtonian fluids, anisotropic viscosity, integral constitutive equation
(18 pages, 2006)

91. A. Winterfeld
Application of general semi-infinite Programming to Lapidary Cutting Problems
Keywords: large scale optimization, nonlinear programming, general semi-infinite optimization, design centering, clustering
(26 pages, 2006)

92. J. Orlik, A. Ostrovska
Space-Time Finite Element Approximation and Numerical Solution of Hereditary Linear Viscoelasticity Problems
Keywords: hereditary viscoelasticity; kern approximation by interpolation; space-time finite element approximation, stability and a priori estimate
(24 pages, 2006)

93. V. Rutka, A. Wiegmann, H. Andrä
EJIIM for Calculation of effective Elastic Moduli in 3D Linear Elasticity
Keywords: Elliptic PDE, linear elasticity, irregular domain, finite differences, fast solvers, effective elastic moduli
(24 pages, 2006)

94. A. Wiegmann, A. Zemitis
EJ-HEAT: A Fast Explicit Jump Harmonic Averaging Solver for the Effective Heat Conductivity of Composite Materials
Keywords: Stationary heat equation, effective thermal conductivity, explicit jump, discontinuous coefficients, virtual material design, microstructure simulation, EJ-HEAT
(21 pages, 2006)

95. A. Naumovich
On a finite volume discretization of the three-dimensional Biot poroelasticity system in multilayered domains
Keywords: Biot poroelasticity system, interface problems, finite volume discretization, finite difference method
(21 pages, 2006)

96. M. Krekel, J. Wenzel
A unified approach to Credit Default Swaption and Constant Maturity Credit Default Swap valuation
Keywords: LIBOR market model, credit risk, Credit Default Swaption, Constant Maturity Credit Default Swap-method
(43 pages, 2006)

97. A. Dreyer
Interval Methods for Analog Circiuts
Keywords: interval arithmetic, analog circuits, tolerance analysis, parametric linear systems, frequency response, symbolic analysis, CAD, computer algebra
(36 pages, 2006)

98. N. Weigel, S. Weihe, G. Bitsch, K. Dreßler
Usage of Simulation for Design and Optimization of Testing
Keywords: Vehicle test rigs, MBS, control, hydraulics, testing philosophy
(14 pages, 2006)

99. H. Lang, G. Bitsch, K. Dreßler, M. Speckert
Comparison of the solutions of the elastic and elastoplastic boundary value problems
Keywords: Elastic BVP, elastoplastic BVP, variational inequalities, rate-independency, hysteresis, linear kinematic hardening, stop- and play-operator
(21 pages, 2006)

100. M. Speckert, K. Dreßler, H. Mauch
MBS Simulation of a hexapod based suspension test rig
Keywords: Test rig, MBS simulation, suspension, hydraulics, controlling, design optimization
(12 pages, 2006)

101. S. Azizi Sultan, K.-H. Küfer
A dynamic algorithm for beam orientations in multicriteria IMRT planning
Keywords: radiotherapy planning, beam orientation optimization, dynamic approach, evolutionary algorithm, global optimization
(14 pages, 2006)

102. T. Götz, A. Klar, N. Marheineke, R. Wegener
A Stochastic Model for the Fiber Lay-down Process in the Nonwoven Production
Keywords: fiber dynamics, stochastic Hamiltonian system, stochastic averaging
(17 pages, 2006)

103. Ph. Süss, K.-H. Küfer
Balancing control and simplicity: a variable aggregation method in intensity modulated radiation therapy planning
Keywords: IMRT planning, variable aggregation, clustering methods
(22 pages, 2006)

104. A. Beaudry, G. Laporte, T. Melo, S. Nickel
Dynamic transportation of patients in hospitals
Keywords: in-house hospital transportation, dial-a-ride, dynamic mode, tabu search
(37 pages, 2006)

105. Th. Hanne
Applying multiobjective evolutionary algorithms in industrial projects
Keywords: multiobjective evolutionary algorithms, discrete optimization, continuous optimization, electronic circuit design, semi-infinite programming, scheduling
(18 pages, 2006)

106. J. Franke, S. Halim
Wild bootstrap tests for comparing signals and images
Keywords: wild bootstrap test, texture classification, textile quality control, defect detection, kernel estimate, nonparametric regression
(13 pages, 2007)

107. Z. Drezner, S. Nickel
Solving the ordered one-median problem in the plane
Keywords: planar location, global optimization, ordered median, big triangle small triangle method, bounds, numerical experiments
(21 pages, 2007)

108. Th. Götz, A. Klar, A. Unterreiter, R. Wegener
Numerical evidance for the non-existing of solutions of the equations desribing rotational fiber spinning
Keywords: rotational fiber spinning, viscous fibers, boundary value problem, existence of solutions
(11 pages, 2007)

109. Ph. Süss, K.-H. Küfer
Smooth intensity maps and the Bortfeld-Boyer sequencer
Keywords: probabilistic analysis, intensity modulated radiotherapy treatment (IMRT), IMRT plan application, step-and-shoot sequencing
(8 pages, 2007)

110. E. Ivanov, O. Gluchshenko, H. Andrä, A. Kudryavtsev
Parallel software tool for decomposing and meshing of 3d structures
Keywords: a-priori domain decomposition, unstructured grid, Delaunay mesh generation
(14 pages, 2007)

111. O. Iliev, R. Lazarov, J. Willems
Numerical study of two-grid preconditioners for 1d elliptic problems with highly oscillating discontinuous coefficients
Keywords: two-grid algorithm, oscillating coefficients, preconditioner
(20 pages, 2007)

112. L. Bonilla, T. Götz, A. Klar, N. Marheineke, R. Wegener
Hydrodynamic limit of the Fokker-Planck-equation describing fiber lay-down processes
Keywords: stochastic dierential equations, Fokker-Planck equation, asymptotic expansion, Ornstein-Uhlenbeck process
(17 pages, 2007)

113. S. Rief
Modeling and simulation of the pressing section of a paper machine
Keywords: paper machine, computational fluid dynamics, porous media
(41 pages, 2007)

114. R. Ciegis, O. Iliev, Z. Lakdawala
On parallel numerical algorithms for simulating industrial filtration problems
Keywords: Navier-Stokes-Brinkmann equations, finite volume discretization method, SIMPLE, parallel computing, data decomposition method
(24 pages, 2007)

115. N. Marheineke, R. Wegener
Dynamics of curved viscous fibers with surface tension
Keywords: Slender body theory, curved viscous bers with surface tension, free boundary value problem
(25 pages, 2007)

116. S. Feth, J. Franke, M. Speckert
Resampling-Methoden zur mse-Korrektur und Anwendungen in der Betriebsfestigkeit
Keywords: Weibull, Bootstrap, Maximum-Likelihood, Betriebsfestigkeit
(16 pages, 2007)

117. H. Knaf
Kernel Fisher discriminant functions – a concise and rigorous introduction
Keywords: wild bootstrap test, texture classification, textile quality control, defect detection, kernel estimate, nonparametric regression
(30 pages, 2007)

118. O. Iliev, I. Rybak
On numerical upscaling for flows in heterogeneous porous media
Keywords: numerical upscaling, heterogeneous porous media, single phase flow, Darcy's law, multiscale problem, effective permeability, multipoint flux approximation, anisotropy
(17 pages, 2007)

119. O. Iliev, I. Rybak
On approximation property of multipoint flux approximation method
Keywords: Multipoint flux approximation, finite volume method, elliptic equation, discontinuous tensor coefficients, anisotropy
(15 pages, 2007)

120. O. Iliev, I. Rybak, J. Willems
On upscaling heat conductivity for a class of industrial problems
Keywords: Multiscale problems, effective heat conductivity, numerical upscaling, domain decomposition
(21 pages, 2007)

121. R. Ewing, O. Iliev, R. Lazarov, I. Rybak
On two-level preconditioners for flow in porous media
Keywords: Multiscale problem, Darcy's law, single phase flow, anisotropic heterogeneous porous media, numerical upscaling, multigrid, domain decomposition, efficient preconditioner
(18 pages, 2007)

122. M. Brickenstein, A. Dreyer
POLYBORI: A Gröbner basis framework for Boolean polynomials
Keywords: Gröbner basis, formal verification, Boolean polynomials, algebraic cryptoanalysis, satisfiability
(23 pages, 2007)

123. O. Wirjadi
Survey of 3d image segmentation methods
Keywords: image processing, 3d, image segmentation, binarization
(20 pages, 2007)

124. S. Zeytun, A. Gupta
A Comparative Study of the Vasicek and the CIR Model of the Short Rate
Keywords: interest rates, Vasicek model, CIR-model, calibration, parameter estimation
(17 pages, 2007)

125. G. Hanselmann, A. Sarishvili
Heterogeneous redundancy in software quality prediction using a hybrid Bayesian approach
Keywords: reliability prediction, fault prediction, non-homogeneous poisson process, Bayesian model averaging
(17 pages, 2007)

126. V. Maag, M. Berger, A. Winterfeld, K.-H. Küfer
A novel non-linear approach to minimal area rectangular packing
Keywords: rectangular packing, non-overlapping constraints, non-linear optimization, regularization, relaxation
(18 pages, 2007)

127. M. Monz, K.-H. Küfer, T. Bortfeld, C. Thieke
Pareto navigation – systematic multi-criteria-based IMRT treatment plan determination
Keywords: convex, interactive multi-objective optimization, intensity modulated radiotherapy planning
(15 pages, 2007)

128. M. Krause, A. Scherrer
On the role of modeling parameters in IMRT plan optimization
Keywords: intensity-modulated radiotherapy (IMRT), inverse IMRT planning, convex optimization, sensitivity analysis, elasticity, modeling parameters, equivalent uniform dose (EUD)
(18 pages, 2007)

129. A. Wiegmann
Computation of the permeability of porous materials from their microstructure by FFF-Stokes
Keywords: permeability, numerical homogenization, fast Stokes solver
(24 pages, 2007)

130. T. Melo, S. Nickel, F. Saldanha da Gama
Facility Location and Supply Chain Management – A comprehensive review
Keywords: facility location, supply chain management, network design
(54 pages, 2007)

131. T. Hanne, T. Melo, S. Nickel
Bringing robustness to patient flow management through optimized patient transports in hospitals
Keywords: Dial-a-Ride problem, online problem, case study, tabu search, hospital logistics
(23 pages, 2007)

132. R. Ewing, O. Iliev, R. Lazarov, I. Rybak, J. Willems
An efficient approach for upscaling properties of composite materials with high contrast of coefficients
Keywords: effective heat conductivity, permeability of fractured porous media, numerical upscaling, fibrous insulation materials, metal foams
(16 pages, 2008)

133. S. Gelareh, S. Nickel
New approaches to hub location problems in public transport planning
Keywords: integer programming, hub location, transportation, decomposition, heuristic
(25 pages, 2008)

134. G. Thömmes, J. Becker, M. Junk, A. K. Vaikuntam, D. Kehrwald, A. Klar, K. Steiner, A. Wiegmann
A Lattice Boltzmann Method for immiscible multiphase flow simulations using the Level Set Method
Keywords: Lattice Boltzmann method, Level Set method, free surface, multiphase flow
(28 pages, 2008)

135. J. Orlik
Homogenization in elasto-plasticity
Keywords: multiscale structures, asymptotic homogenization, nonlinear energy
(40 pages, 2008)

136. J. Almquist, H. Schmidt, P. Lang, J. Deitmer, M. Jirstrand, D. Prätzel-Wolters, H. Becker
Determination of interaction between MCT1 and CAII via a mathematical and physiological approach
Keywords: mathematical modeling; model reduction; electrophysiology; pH-sensitive microelectrodes; proton antenna
(20 pages, 2008)

137. E. Savenkov, H. Andrä, O. Iliev
An analysis of one regularization approach for solution of pure Neumann problem
Keywords: pure Neumann problem, elasticity, regularization, finite element method, condition number
(27 pages, 2008)

138. O. Berman, J. Kalcsics, D. Krass, S. Nickel
The ordered gradual covering location problem on a network
Keywords: gradual covering, ordered median function, network location
(32 pages, 2008)

139. S. Gelareh, S. Nickel
Multi-period public transport design: A novel model and solution approaches
Keywords: Integer programming, hub location, public transport, multi-period planning, heuristics
(31 pages, 2008)

140. T. Melo, S. Nickel, F. Saldanha-da-Gama
Network design decisions in supply chain planning
Keywords: supply chain design, integer programming models, location models, heuristics
(20 pages, 2008)

141. C. Lautensack, A. Särkkä, J. Freitag, K. Schladitz
Anisotropy analysis of pressed point processes
Keywords: estimation of compression, isotropy test, nearest neighbour distance, orientation analysis, polar ice, Ripley's K function
(35 pages, 2008)

142. O. Iliev, R. Lazarov, J. Willems
A Graph-Laplacian approach for calculating the effective thermal conductivity of complicated fiber geometries
Keywords: graph laplacian, effective heat conductivity, numerical upscaling, fibrous materials
(14 pages, 2008)

143. J. Linn, T. Stephan, J. Carlsson, R. Bohlin
Fast simulation of quasistatic rod deformations for VR applications
Keywords: quasistatic deformations, geometrically exact rod models, variational formulation, energy minimization, finite differences, nonlinear conjugate gradients
(7 pages, 2008)

144. J. Linn, T. Stephan
Simulation of quasistatic deformations using discrete rod models
Keywords: quasistatic deformations, geometrically exact rod models, variational formulation, energy minimization, finite differences, nonlinear conjugate gradients
(9 pages, 2008)

145. J. Marburger, N. Marheineke, R. Pinnau
Adjoint based optimal control using mesh-less discretizations
Keywords: Mesh-less methods, particle methods, Eulerian-Lagrangian formulation, optimization strategies, adjoint method, hyperbolic equations
(14 pages, 2008

146. S. Desmettre, J. Gould, A. Szimayer
Own-company stockholding and work effort preferences of an unconstrained executive
Keywords: optimal portfolio choice, executive compensation
(33 pages, 2008)

147. M. Berger, M. schröder, K.-H. Küfer
A constraint programming approach for the two-dimensional rectangular packing problem with orthogonal orientations
Keywords: rectangular packing, orthogonal orientations non-overlapping constraints, constraint propagation
(13 pages, 2008)

148. K. Schladitz, C. Redenbach, T. Sych, M. Godehardt
Microstructural characterisation of open foams using 3d images
Keywords: virtual material design, image analysis, open foams
(30 pages, 2008)

Status quo: October 2008